

UNIVERSITY OF READING
School of Mathematics, Meteorology and Physics

DOES SELF-ORGANISED CRITICALITY OCCUR
IN THE TROPICAL CONVECTIVE SYSTEM?

TOM JORDAN

August 2008

This dissertation is submitted to the Department of Mathematics and the Department of Meteorology in partial fulfilment of the requirements for the degree of Master of Science

Abstract

Self-organised criticality (SOC) is a theory of the underlying dynamics of a class of non-equilibrium dynamical systems that are associated with complex, scale-free phenomena. Recently, there has been growing empirical evidence proposed that links the Tropical Convective System (TCS) to SOC. This has broad implications for both the theory of SOC and the understanding of the underlying nature of the dynamics of convection.

As of now, there has not been a simple model devised for the TCS that is able to anticipate the scale-free phenomena that occurs. In this exploratory study we identify the dynamical features of the TCS that are suspected to relate to a self-organised critical system, highlighting cold-pools as the prominent organisation mechanism. We then adapt and extend an existing SOC model to formulate the dynamics of the TCS as cellular automation process.

Our numerical simulation produces examples of both spatial and temporal power-law relationships in a region of parameter space that is physically close to what can be associated with the TCS. We show that our model is robust to simple modifications, which has important consequences for its application to physical reality. The model is however, unable to directly reproduce the current empirical evidence for SOC in the TCS. We conclude that for this to be fully realised, a future model must be devised with a specific meteorological diagnostic in mind.

Acknowledgements

Firstly, I would like to thank my supervisor Dr. Robert Plant. His enthusiasm, encouragement and insightful discussions have made the project a pleasure to work on. On the administrative side of things, I would like to thank Dr. Peter Sweby and Sue Davis for looking after us throughout the year.

As always, I would like to thank my family for their ongoing love and support in everything that I do. A special mention must also go to the 'room 105 crew', whose combination of chocolate Minstrels, Kinder eggs, caffeine and duck balloons kept it fun. Thanks must also go to any individual who has helped me with my understanding and appreciation of maths and physics over the years leading up to this project: in particular, my A-level physics teacher Mr. G, who helped me realise that the natural world was fascinating and beautiful in the first place!

Finally, I would like to acknowledge the financial support of the Royal Meteorological Society that has enabled me to complete this Master of Science degree.

Declaration

I confirm that this is my own work and the use of all material from other sources has been properly and fully acknowledged.

Signed Date

Contents

1	Introduction	1
1.1	Complexity and self-organised criticality	1
1.2	The tropical convective system: a meteorological application of SOC? . . .	2
1.3	Report structure	3
2	Self-organised criticality	4
2.1	Scale-free behaviour	4
2.1.1	Power-law relationships, scale-invariance and fractals	4
2.1.2	$1/f$ behaviour	6
2.2	The theory of self-organised criticality	7
2.2.1	Statistical mechanical background	7
2.2.2	The application of SOC to natural systems	8
2.2.3	Numerical simulation and mathematical formalism	9
2.3	The OFC earthquake model	10
2.3.1	Empirical motivation	11
2.3.2	Development from basic physics	11
2.3.3	Numerical simulation	12
2.4	The consequences of Chapter 2 for the project	14
3	The case for self-organised criticality in the tropical convective system	16
3.1	Convection in the tropics	16

3.1.1	Meteorological scales	16
3.1.2	Convective clouds and organisational structures	17
3.1.3	The quasi-equilibrium hypothesis	18
3.2	Observational studies	19
3.2.1	European rainfall statistics	19
3.2.2	1/f behaviour in the Pacific	20
3.2.3	Critical phenomena in tropical rain	21
3.3	The consequences of Chapter 3 for the project	22
4	Model physics	24
4.1	Atmospheric physics background	24
4.1.1	Atmospheric composition and equation of state	25
4.1.2	Saturation	25
4.1.3	Atmospheric stability	26
4.1.4	Static energy and its relation to atmospheric lapse rates	28
4.1.5	Mean tropospheric profiles	29
4.2	Threshold model	30
4.2.1	Stability properties of the three level model	30
4.2.2	Forcing	31
4.2.3	Level budget equations and solutions	32
4.2.4	Evolution toward a threshold	33
4.3	Relaxation and interaction mechanisms	36
4.3.1	The life cycle of a convective cell and its relation to cold pool formation	36
4.3.2	Consequences of the cold pool for the model	37
4.4	Summary and development of model physics	38
4.4.1	Dynamical features of the TCS	38
4.4.2	Time-scales in the TCS	39
4.4.3	Steps toward a cellular automation model of the TCS	40

5	A cellular automation model of the tropical convective system	42
5.1	The development of the model	42
5.1.1	Model overview and terminology	43
5.1.2	The cellular automation algorithm	43
5.1.3	Relation to model physics	45
5.2	Model testing	46
5.2.1	Relationship to the forest-fire models	46
5.2.2	Is the model critical?	47
5.2.3	Scale-invariant diagnostics	49
5.2.4	Comparison between simulation results	49
5.3	Simulation results in a meteorological region of parameter space	51
5.4	Relaxation parameterisations	53
5.4.1	Relaxation to fixed value and hybrid	54
5.4.2	Relaxation to a stochastic value and hybrid	54
5.5	System size investigation	56
5.6	Summary of results	57
6	Summary, future work and conclusions	60
6.1	Summary and discussion	60
6.2	Future work	62
6.3	Conclusions	63
A	Model Simulation	65
A.1	Overview	65
A.2	Data sampling	65

List of Figures

2.1	(a) City population against rank [11] - (double-logarithmic scale), (b) Koch snowflake fractal [12]	5
2.2	(a) Classes of time signal: $\alpha = 0$ (upper), $\alpha = 1$ (centre), $\alpha = 2$ (lower), [7], (b) $1/f$ power spectrum from classical music signal [13]	6
2.3	(a) Sand-pile conceptual model [1], (b) Rice-pile experiment [16]	9
2.4	The Gutenberg-Richter law for earthquakes: (a) Empirical data set [19], (b) Numerical simulation [18], (both double-logarithmic scale)	11
2.5	A schematic diagram of the OFC spring-block earthquake model [18]	12
2.6	The OFC earthquake model cellular automation iteration process	13
3.1	Convective clouds: (a) Shallow cumulus, (b) Mature deep cumulus [20]	18
3.2	Rain event power-law relationships: (a) Number density of rain events against event size, (b) Number density of rain event duration against versus event duration, (both double logarithmic scale)	20
3.3	TOGA-COARE data from site in mid-Pacific: (a) Time series, (b) Power spectra, for: air temperature T_{air} , moisture mixing ratio q , wind speed $ \mathbf{v} $ and rain rate R , [7]	21
4.1	Mean tropical tropospheric profiles for s , h and h^* [30]	29
4.2	Evolution of h and h^* over the interval $t \in [0, 24\text{hrs}]$	34
4.3	(a) Vertical profiles of h and h^* at $t = 0$ and $t = 16$ hrs, (b) Evolution of H over the interval $t \in [0, 24\text{hrs}]$	35

4.4	Schematic diagram of cold pool development and the associated T_1 and q_1 perturbations in the boundary layer [9]	37
4.5	Image of mean annual deep convective cloud cover percentage [33]	40
5.1	The tropical convection cellular automation iteration process with periodic boundary conditions over 9 iteration steps	45
5.2	Evolution of a/b for: $A_C = 1.0$, $A_R = 1.0$, $A_P = 0.0$: (a) $\delta A = 10^{-3}$, (b) $\delta A = 10^{-4}$	48
5.3	Results for ‘critical regime’: $\delta A = 10^{-4}$, $A_C = 1.0$, $A_R = 1.0$, $A_P = 0$: $a/b \approx 0.08$, $b \approx 10^{-4}$	50
5.4	(a) $\log(S_Q)$ against $\log(f_Q)$, (b) $\log(P_Q)$ against $\log(r_Q)$ [34]	51
5.5	Results for typical meteorological parameter set: $\delta A = \frac{1}{32}$, $A_C = 1.0$, $A_R = 1.0$, $A_P = 0.5$: $a/b \approx 0.1$, $b \approx 0.03$	52
5.6	Results for lower bound upon time-scale separation: $\delta A = \frac{1}{96}$, $A_C = 1.0$, $A_R = 1.0$, $A_P = 0.5$: $a/b \approx 0.1$, $b \approx 0.01$	53
5.7	Results for relaxation to a fixed value: $\delta A = \frac{1}{96}$, $A_C = 1.0$, $A_R = 1.0$, $A_C = 0.5$	54
5.8	Results for relaxation to stochastic value: $\delta A = \frac{1}{96}$, $A_C = 1.0$, $A_R = 1.0$, $A_P = 0.5$: $a/b \approx 0.08$, $b \approx 0.01$	55
5.9	Results for relaxation to stochastic-hybrid value: $\delta A = \frac{1}{96}$, $A_C = 1.0$, $A_R = 1.0$, $A_P = 0.5$: $a/b \approx 0.07$, $b \approx 0.01$	56
5.10	System size plots for $\log(r_Q)$ against $\log(P_Q)$: $L = 250$, $L = 50$, $L = 10$	57
6.1	Results for q_1 : $\delta A = \frac{1}{32}$, $A_C = 1.0$, $A_R = 1.0$, $A_P = 0.5$: (a) Simulation time series for q_1 , (b) $\log(S_{q_1})$ against $\log(f_{q_1})$	64

Symbols, constants and acronyms

Atmospheric physics symbols

Symbol	Units	Description
p	kPa	Pressure
ρ	Kgm^{-3}	Density
T	K	Temperature
e	Pa	Water vapour partial pressure
e^*	Pa	Saturation water vapour partial pressure
q	gkg^{-1}	Mixing ratio
q^*	gkg^{-1}	Saturation mixing ratio
H	-	Relative humidity
f_b	N	Buoyancy force
z	km	Vertical height coordinate
N	s^{-1}	Buoyancy frequency
s	Jkg^{-1}	Static energy
h	Jkg^{-1}	Moist static energy
h^*	Jkg^{-1}	Saturation moist static energy
$ \mathbf{v} $	ms^{-1}	Wind speed
Γ	Kkm^{-1}	Atmospheric lapse rate
F_r	$\text{Jkg}^{-1}\text{s}^{-1}$	Radiative forcing
F_s	$\text{Jkg}^{-1}\text{s}^{-1}$	Surface energy flux
F_q	s^{-1}	Surface moisture flux

Constants

Symbol	Value	Description
R_d	$287 \text{ Jkg}^{-1}\text{K}^{-1}$	Gas constant for dry air
R_v	$462 \text{ Jkg}^{-1}\text{K}^{-1}$	Gas constant for water vapour
L_v	$2.50 \times 10^6 \text{ Jkg}^{-1}$	Latent heat of water
c_p	$1010 \text{ Jkg}^{-1}\text{K}^{-1}$	Specific heat capacity of dry air at constant pressure
g	9.81 ms^{-2}	Gravitational acceleration

Convection model symbols

Symbol	Description
A	Age
A_C	Auto-convection threshold age
A_P	Inter-convection threshold age
A_R	Relaxation reset age
δA	Age increment
κ	Fixed reset value
X	Stochastic reset value
L	Lattice size index
n_Q	Number of quiescent sites
f_Q	Frequency of quiescent sites
S_Q	Power spectrum of quiescent sites
r_Q	Size of cluster of quiescent sites

Acronymns

SOC	Self-Organised Criticality
DOF	Degree Of Freedom
TCS	Tropical Convective System
OFC	Olami, Feder, Christensen
QE	Quasi Equilibrium
DFE	Deterministic Forest Fire
SFF	Stochastic Forest Fire

Chapter 1

Introduction

1.1 Complexity and self-organised criticality

A complex system is composed of many degrees of freedom (DOF) which through mutual interaction produce emergent behaviour that is not predicted from the individual behaviour of the DOF alone. The emergent behaviour is referred to as ‘complex’ due to having large variability and lacking a characteristic response size [1]. This variability can apply both spatially and temporally and is mathematically connected to *scale-invariant* phenomena: fractal structures (space) and $1/f$ behaviour (time).

Self-organised criticality (SOC) was introduced as universal mechanism that could in principle explain how emergent complex behaviour arises [2]. It is a theory of the *underlying dynamics* of a class of systems that all share a very general, characteristic behaviour. SOC deals with *slowly driven* systems that exhibit *threshold* behaviour and *interaction* between their DOF. The scope of the theory of SOC is incredibly broad. Examples of its application include avalanches in granular piles, earthquakes in seismic systems, and (perhaps more speculatively!) extinctions and mutations in biological evolution [1].

The theoretical foundations of the subject are linked to an area of physics that is well understood; the statistical mechanics of critical phenomena and continuous phase transitions [3]. There is however, a lack of a general mathematical formalism for SOC, and the non-equilibrium systems that it deals with are less well understood than equilibrium systems [4]. The SOC approach has also been criticised because it neglects many of the

specific details of the systems it has been applied to and produces very general statistical statements rather than precise predictions [1]. Nevertheless, if viewed as trying to answer the question: ‘How and why does complex behaviour arise?’, not: ‘What will a particular outcome be?’, then SOC is a compelling framework to apply.

1.2 The tropical convective system: a meteorological application of SOC?

The atmosphere is one of the most well observed and measured natural systems. Since the mid 1990s there has been growing evidence that a broad range of atmospheric phenomena exhibit wide variability and scale-free behaviour [5], [6]. This contrasts with the traditional meteorological viewpoint, where characteristic scales are assumed to be linked to specific phenomena. In recent years, the Tropical Convective System (TCS) has been isolated as a prominent example of this, with time-series of convective events exhibiting $1/f$ behaviour [7], and power-law relationships identified in satellite data for tropical rain [8].

The dynamics of the TCS contain many features that are potentially identifiable with SOC. The TCS is slowly driven through long-wave radiative cooling, surface heating and evaporation which leads to conditional instability (a dynamical threshold), and the onset of convection. Convective events occur over a wide range of spatial and temporal scales, ranging from isolated storms that last for less than an hour to meso-scale convective clusters which span for hundreds of kilometres and last for days at a time. The underlying organisational mechanisms of the TCS are much debated, with some recent work emphasising short range thermodynamical interactions that are linked to the formation of a ‘cold-pool’ following a deep convective event [9].

SOC could potentially provide the underlying framework, that unites the observations of scale-free phenomena and the non-equilibrium dynamical features of the TCS. As of now, there has not been a simple model devised for the TCS that is able to anticipate the scale-free phenomena which occurs [8]. The central aim of this project is to identify the features of the TCS that could potentially relate to a self-organised critical dynamical system and then use these features to construct a phenomenological model.

1.3 Report structure

The report structure is outlined below:

- Chapter 2 outlines the theory of SOC and its relationship to scale-free behaviour. The application of SOC to the seismic system is used to clarify what can be expected of the application of SOC to a ‘real world’ system.
- Chapter 3 outlines the empirical evidence for why the TCS is considered as a good candidate for exhibiting elements of self-organised critical behaviour. A qualitative overview is provided of the main dynamical features of the TCS.
- Chapter 4 identifies more precisely the features of the TCS that are suspected to be linked to SOC. This is done using atmospheric physics principles.
- Chapter 5 develops a simple numerical model of the TCS based upon an existing SOC algorithm. Scale-invariant diagnostics are explored in what is deemed to be a meteorological limit.
- Chapter 6 concludes the project and proposes future directions of study.

SOC is a largely unfamiliar concept to most meteorologists, and the details of the TCS are largely unfamiliar to most mathematicians. However, this project endeavours to be as self-contained as possible. Chapters 2 and 3 are primarily a literature review and Chapters 4 and 5 contain the majority of the original work.

Chapter 2

Self-organised criticality

SOC was introduced in 1987 by Bak, Tang and Weissenfeld [2] as an explanation of how scale-free behaviour can arise in a class of non-equilibrium dynamical systems. Scale-free behaviour is certainly not unique to SOC, and the first section of this chapter outlines what is meant by this. SOC is then introduced, using a sand-pile to illustrate the key dynamical features. The simulation and mathematical formalism of self-organised critical systems is discussed. Finally, the seismic system is used as a ‘case-study’ to illustrate the application of SOC to a ‘real world’ physical system.

2.1 Scale-free behaviour

2.1.1 Power-law relationships, scale-invariance and fractals

Empirical power-law relationships arise in a broad variety of natural and man-made phenomena. Examples include earthquake magnitudes, city population sizes and fossil extinction records [1]. A power-law relationship is defined as polynomial relationship of the form

$$p(x) \propto x^{-\alpha}, \tag{2.1}$$

where $\alpha \in \mathbb{R}$ is the exponent or scaling parameter [10]. Frequently $p(x)$ is a probability density function, and $\alpha > 1$ is required for the distribution to be normalisable. Power laws have the property that they are *scale-invariant*. This can be seen by making the scaling

transformation $p(x) \rightarrow p(\lambda x)$ where $\lambda \in \mathbb{R}$ is a scale factor. The relationship

$$p(\lambda x) = \lambda^{-\alpha} p(x), \quad (2.2)$$

follows. This is interpreted as a rescaling of $p(x)$ that is independent of x . A power-law relationship therefore lacks a characteristic scale. ‘Scale-free behaviour’ is generally understood to be less strict than the relationship (2.2), and corresponds to approximate scale-invariant behaviour in empirical (or simulation) data sets.

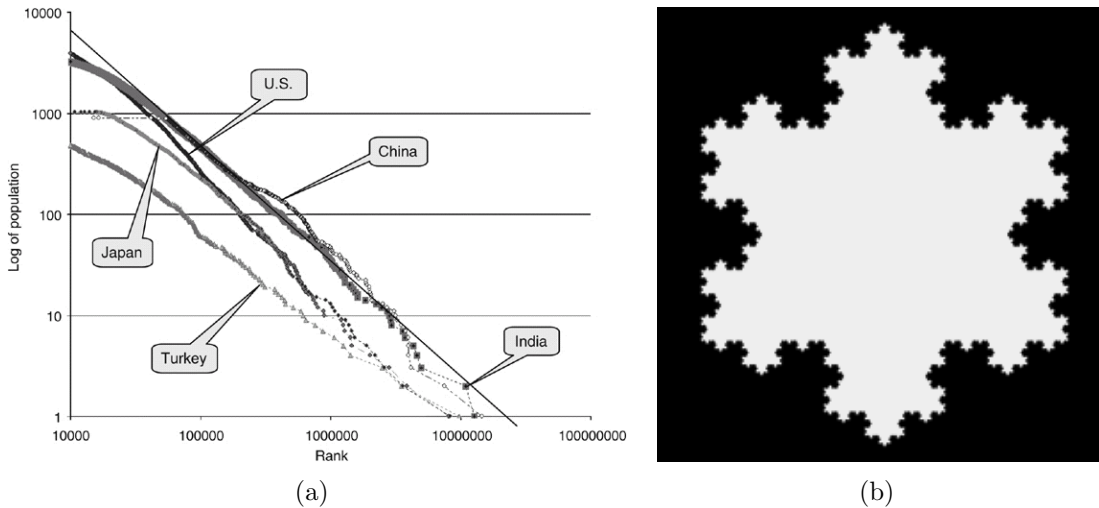


Figure 2.1: (a) City population against rank [11] - (double-logarithmic scale), (b) Koch snowflake fractal [12]

It follows from (2.1) that a power-law corresponds to a straight line on a double logarithmic plot with the gradient being $-\alpha$. A double logarithmic plot of city population against size rank for cities in 5 different countries is shown in Figure 2.1(a) and illustrates this point. In practice, discerning if a data set strictly follows a power-law is a highly complicated procedure. Problems can arise through applying standard linear regression techniques and analysing the tail of the data [10].

The fractal dimension of an object can often be related to the exponent of a power law. An example is the Koch snowflake curve (Figure 2.1(b)) which has a fractal dimension given by $L_n = (\frac{4}{3})^n$ where L_n is the length of a line segment after n magnifications [12]. Spatial power-laws are therefore often referred to as ‘fractal behaviour’ and this is used concurrently in the SOC literature.

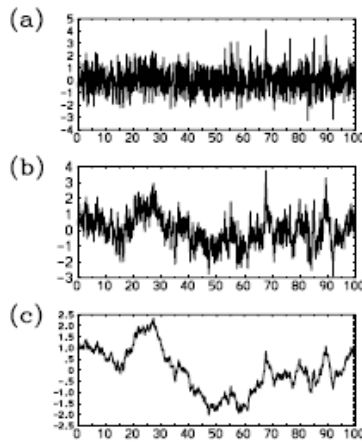
2.1.2 $1/f$ behaviour

Experimental data that is recorded at discrete intervals over an extended period of time can be recorded as a time-series $\Lambda(t)$. Examples from meteorology include air temperature and precipitation. Applying harmonic analysis, the power spectrum $S(f)$ is defined by the square of the Fourier transform of $\Lambda(t)$

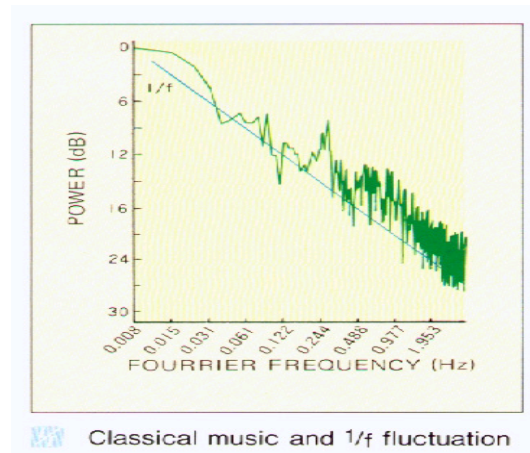
$$S(f) = \lim_{\tau \rightarrow \infty} \frac{1}{2\tau} \left| \int_{-\tau}^{\tau} \Lambda(t) \exp(i2\pi ft) dt \right|^2, \quad (2.3)$$

where τ is the time period. As observational data is recorded over a finite interval, an approximation is made when taking the limit $\tau \rightarrow \infty$. It is an observed fact that many natural systems have power spectra that exhibit a power-law regime of the form $S(f) \propto f^{-\alpha}$. Figure 2.2(a) shows 3 important classes of power-law time signals that frequently arise in natural systems. The signals correspond to:

1. $\alpha = 0$: *White behaviour* - ‘Random, uncorrelated fluctuations about a mean value’
2. $\alpha = 1$: *$1/f$ behaviour* - ‘Noisy, pulse like episodes embedded in quieter periods’
3. $\alpha = 2$: *Brownian behaviour* - ‘Correlated, experiencing drifting tendencies’ [7]



(a)



(b)

Figure 2.2: (a) Classes of time signal: $\alpha = 0$ (upper), $\alpha = 1$ (centre), $\alpha = 2$ (lower), [7], (b) $1/f$ power spectrum from classical music signal [13]

Analysis of $1/f$ signal behaviour shows that the statistical correlations between different points in time do not exist. A simple argument for why this is the case considers the Fourier transform of the auto-correlation function $G(t)$ of a stationary time signal [4]. This is given by

$$G(t) = \lim_{\tau \rightarrow \infty} \frac{1}{\tau} \int_0^\tau \Lambda(t_0)\Lambda(t_0 + t)dt_0,$$

where the corresponding Fourier transform relation (neglecting normalisation factors) is

$$S(f) = \lim_{\tau \rightarrow \infty} \int_0^\tau G(t) \cos(2\pi ft)dt. \quad (2.4)$$

It is then assumed that power-law relationships of the form; $S(f) \sim f^{-\alpha}$ and $G(t) \sim t^{-\beta}$ exist. Making the substitution $x = 2\pi ft$ into (2.4) gives the result

$$f^{-\alpha} \sim f^{(\beta-1)} \lim_{\tau \rightarrow \infty} \int_0^\tau x^{-\beta} \cos(x)dx,$$

and assuming that the integral converges it follows that $f^{-\alpha} \sim f^{(\beta-1)}$. For β close to 0 α is close to 1 and the power spectrum is thus close to $S(f) \sim f^{-1}$. This corresponds to long time correlations, as the assumed form of $G(t)$ corresponds to a slow fall-off. This is interpreted that no characteristic time-scale to $\Lambda(t)$ exists and $1/f$ behaviour is therefore often referred to as a ‘fractal in time’. For the special case of $\beta = 0$, $\alpha = 1$ this argument breaks down and details are given in [4].

Scientists from many disciplines are interested in $1/f$ behaviour as it is a ubiquitous natural phenomena. Examples include the flow of the river Nile, the luminosity of stars and classical music (shown in Figure 2.2(b)), [1]. Frequently it can be difficult to distinguish true signals from a background noise and power spectra with $\alpha \in [0.8, 1.4]$ is often taken as a practical definition of $1/f$ behaviour by experimental and observational scientists [14].

2.2 The theory of self-organised criticality

2.2.1 Statistical mechanical background

The term ‘*criticality*’ originates from equilibrium statistical mechanics and is connected to continuous phase transitions. Continuous phase transitions are governed by the concept of universality which unites seeming unrelated systems such as magnets and superconductors

under the same theoretical framework. The critical point of a phase transition is reached by precise ‘tuning’ of a control parameter, (frequently temperature), and is characterised by a scale-free response to perturbation. This amounts to the system exhibiting a different response when perturbed at different regions at different times - the dynamics of the system are global and an ‘average system-response’ does not exist [3].

In statistical mechanics ‘*self-organisation*’ refers to the ability of certain non-equilibrium systems to develop structures and patterns in the absence of significant control or tuning by an external agent. SOC refers to self-organising systems exhibiting an analogue to the critical behaviour observed during a continuous phase transition. The difference being is that a SOC system does not require precise external tuning to reach the critical point - rather, the critical state is reached through the mutual interaction of the DOF in the system [4].

2.2.2 The application of SOC to natural systems

A sand-pile was one of the first systems that was proposed to exhibit self-organised critical behaviour. It was thought to represent the canonical form of the dynamical features of an SOC system and was used to illustrate the key principles of the theory [1], [2]. Figure 2.3(a) is a schematic diagram of the sand-pile system, described below:

- The sand-pile is ‘driven’ by adding grains of sand one by one at random positions.
- Due to friction, the grains get stuck upon impact and form a ‘landscape’ consisting of slopes of varying angles.
- Avalanches occur when the local slope exceeds a threshold value, resulting in a transfer of grains to neighbouring regions and dissipation at the boundary.
- Upon repeated addition of grains, the sand-pile proceeds to evolve toward a steady state where the addition of grains is balanced by dissipation at the boundary.
- In this state, (the ‘critical state’), avalanches of all sizes can occur. The dynamics of the system is global and well defined statistical laws that are emergent properties of the system arise.

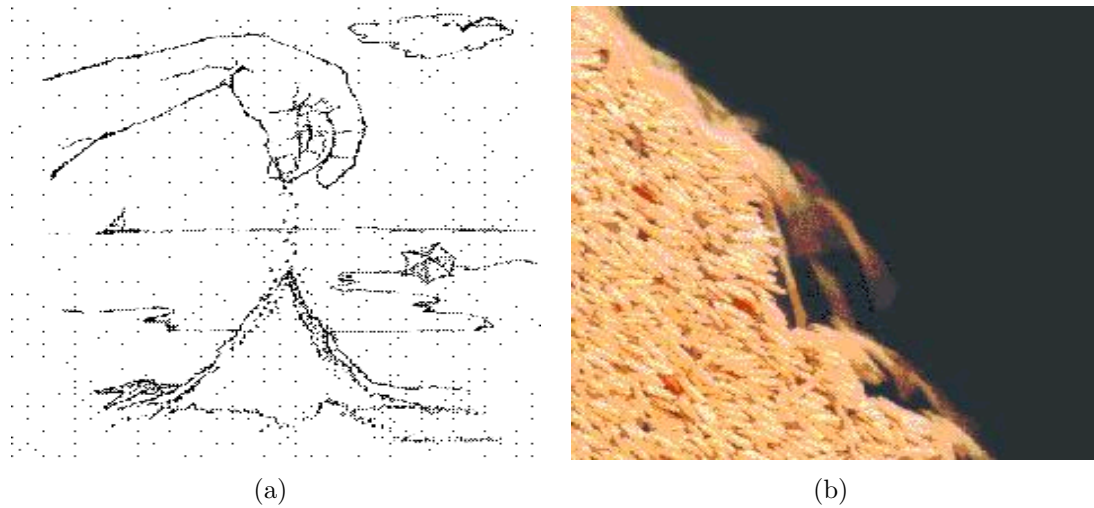


Figure 2.3: (a) Sand-pile conceptual model [1], (b) Rice-pile experiment [16]

It is a necessary condition for SOC that a system is able to produce both a temporal power law relationship (generally $1/f$ behaviour) and a spatial power law. In the case of the sand-pile, $1/f$ behaviour arises from the time series of avalanche sizes and a spatial power law relationship arises from considering the probability of an avalanche being of a given radial extent [4]. A further characteristic of an SOC system is a *time-scale separation* between periods of slow drive and fast pulse-like energy release. In the case of the sand-pile this corresponds to the time-scale separation between grains being slowly added and stored as potential energy in the system, and the fast release of kinetic energy in an avalanche.

The original sand-pile system was a numerical simulation. In reality, sand-piles have insufficient friction to reach the critical state. However, experiments performed upon ricepiles show that a critical state emerges [15]. Figure 2.3(b) demonstrates how the static friction between rice grains is sufficient to produce a build up of potential energy in the system, thus allowing for large avalanches to occur. Due to the simplicity of the conceptual sand-pile argument and the success of the rice-pile experiment, granular piles now stand as a metaphor for the theory of SOC [4].

2.2.3 Numerical simulation and mathematical formalism

SOC systems are typically modelled using a cellular automation algorithm. This consists of a set of grid cells that evolve through a number of discrete iterations according to a set of simple rules. These rules are based both upon a global driving property and

the states of neighbouring cells. Cells represent the DOF of the system and store a ‘dynamic variable’, (such as the height of a granular column). Complexity arises through the repeated application of the simple rules applied to many DOF, rather than complicated behaviour of the DOF in isolation.

There is a degree of variation in the models that have successfully been shown to exhibit SOC, with both stochastic and deterministic automata algorithms obtaining a critical state. In addition, a SOC model can exhibit a degree of internal dissipation and the dynamic variable does not always have to be conserved. There is however, a limited number of automata algorithms that have been discovered which exhibit SOC. Due to this limitation, the development of a model often precedes an application. An example of this is the ‘stochastic forest fire model’ which was proposed in abstraction from any real-world application and has since been used to model disease epidemics [17].

In contrast with equilibrium statistical mechanics a general mathematical formalism has not been developed (or does not exist) with which the behaviour of SOC systems can be analysed. Nevertheless, analytic approaches specific to a given system have been developed which have greatly aided understanding and increased the credibility of the field. For example, an analytic approximation of the sand-pile algorithm has shown that the criticality that is observed is not a result of simulations on a system of a finite size [4].

The analytic approximations are often constructed using a *mean-field* approach. This amounts to approximating the discrete cellular automata by a set of equations of motion that is reminiscent of the continuum limit applied in fluid dynamics. The hope is that a mean-field approach is qualitatively, rather than quantitatively correct [4].

2.3 The OFC earthquake model

It is a widely held view that the seismic system is one of the most successful applications of SOC to date. Motivated by an empirical power-law, a cellular automation model based upon the dynamics of an earthquake fault was developed by Olami, Feder and Christensen [18], (from herein OFC). This section summarises the key results and development stages of the study.

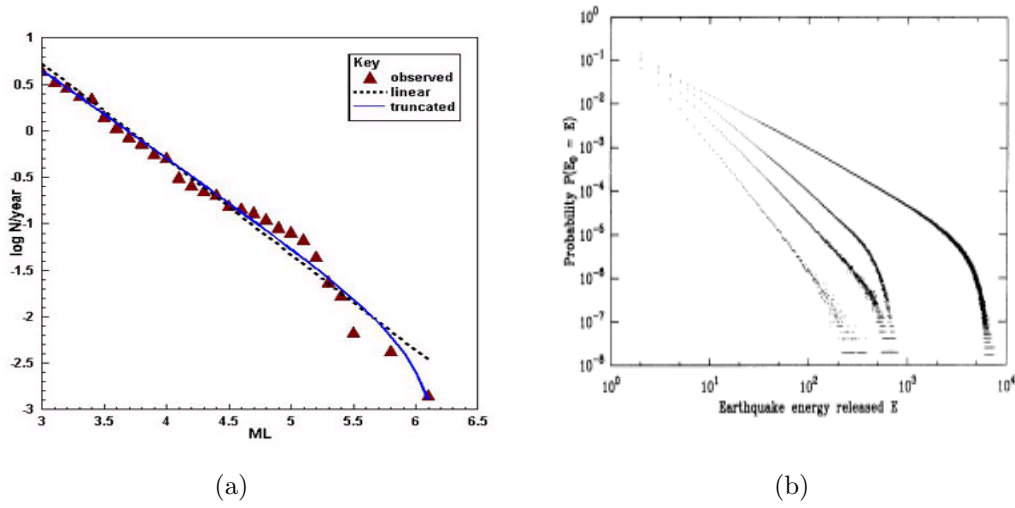


Figure 2.4: The Gutenberg-Richter law for earthquakes: (a) Empirical data set [19], (b) Numerical simulation [18], (both double-logarithmic scale)

2.3.1 Empirical motivation

The Gutenberg-Richter law is a statistical statement that expresses the relationship between the magnitude and total number of earthquakes in a given region over a fixed time period. A well defined power-law relationship is observed, with the number of earthquakes n of energy E greater than a fixed energy E_0 given by $n(E > E_0) \propto E_0^{-\beta}$ where β is a non-integral exponent [18]. Figure 2.4(a) illustrates this relationship for earthquakes in the United Kingdom. Earthquakes, therefore can be viewed as not possessing a characteristic size. The SOC approach to the seismic system provides the underlying framework to explain this.

2.3.2 Development from basic physics

The OFC earthquake model is an idealisation of the dynamical processes that occur in an earthquake fault zone. The simplifications that are made seek to capture the essence of the basic phenomena whilst disregarding any features that over complicate the model. Figure 2.5 is a schematic of this physical idealisation. A summary of the steps that are taken in reaching this is as follows:

- The initial picture is complicated. Convection currents beneath the Earth's crust cause tectonic plates to move relative to each other that in turn cause strain to build up in a boundary region (the fault). This strain is released as an earthquake.
- An idealisation is made. The fault is represented by a 2D network of coupled spring-block oscillators which constitute the DOF of the system.
- These spring-blocks are driven by the relative motion of two rigid planar surfaces, that represent the boundaries between the fault and the adjacent tectonic plate.
- Equations of motion are then derived from the strain force exerted upon each block.
- The initiation of a quake is defined by the force on a block exceeding a threshold value, resulting in a block slipping and transfer of momentum to neighbouring blocks. A chain reaction may result until the system of blocks fully relaxes.

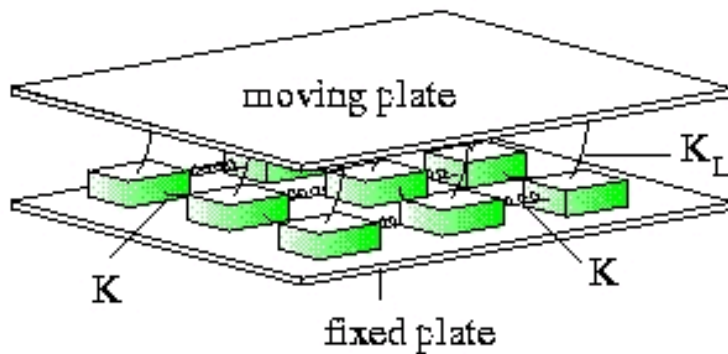


Figure 2.5: A schematic diagram of the OFC spring-block earthquake model [18]

2.3.3 Numerical simulation

From the spring-block model a cellular automation algorithm using the force on each spring-block F_{ij} as a dynamical variable is developed. The model is defined upon a $L \times L$ lattice indexed by (i,j) . Lattice vertices are block centres and forces are stored in a matrix \underline{F} . The algorithm sequence is defined as follows, [4], [18]:

Initialisation:

- Random, uniformly distributed initial forces $F_{ij} \in [0, F_c)$ are assigned to each block where F_c is a threshold force.

Drive:

- System is globally perturbed: $F_{ij} \longrightarrow F_{ij} + \nu, \forall ij$ where ν is an increment of force.

Threshold, relaxation and interaction:

- Test if $F_{ij} > F_c$ - if so then: $F_{ij} \longrightarrow 0$ and $F_{i\pm 1j} \longrightarrow F_{i\pm 1j} + \mu F_{i\pm 1j}$ and $F_{ij\pm 1} \longrightarrow F_{ij\pm 1} + \mu F_{ij\pm 1}$ where $\mu \in (0, 0.25]$ determines the level of conservation.
- Repeat until $F_{ij} \leq F_c, \forall ij$. Once condition is met, re-drive system.

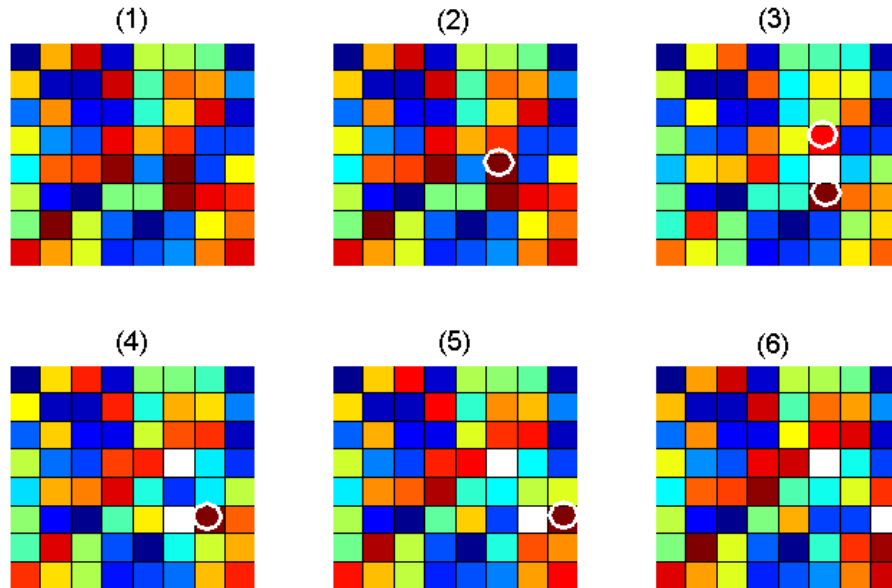


Figure 2.6: The OFC earthquake model cellular automation iteration process

In order to gain an insight toward simulating SOC systems, we reproduced the OFC algorithm. A sequence of output slides is shown in Figure 2.6. Slide 1 corresponds to the system in a sub-threshold state - (warmer colours correspond to higher values of F_{ij}). The system is driven by identifying the greatest value of F_{ij} and then globally perturbing the system by an increment ν that makes this site above threshold. This is shown in slide 2 with the above threshold block notated by a circle. Slide 3 shows relaxation to zero (notated by white), of the above threshold block and the transfer of force to nearest neighbours. (The conservation parameter $\mu = 0.20$ was used in the simulation). Nearest neighbours that are now above threshold are notated by a circle. These in turn relax in slide 4. Slides 5-6 demonstrate how this process is repeated until all blocks are sub-threshold.

The energy of a quake is defined as being proportional to the number of individual relaxations per global perturbation. In this case the energy is 5 units. With the exception of initialisation, the model is fully deterministic. Open boundary conditions are implemented. Physically this corresponds to momentum being dissipated at the boundaries of the fault. Periodic boundary conditions have been experimented with for the OFC model, with the notable result that this removes the criticality of the system [4].

The simulations used by OFC were typically on a system size $L^2 \in [10^3, 10^4]$ and are able to reproduce the Gutenberg-Richter law. This is shown in Figure 2.4(b). The different lines correspond to different system sizes. The ‘cut-off’ at high energies is a typical feature of a SOC simulation and is related to the finite size of the model. The model is viewed as being one of the most robust SOC algorithms and can even predict features such as regional variation in the exponent of the power-law relationship [18].

2.4 The consequences of Chapter 2 for the project

SOC is a broad field of research, spanning mathematics, physics and computer science departments around the world. Different research groups concentrate upon different aspects of the theory, ranging from abstract mathematical formalism, to analysing empirical data sets.

This project is particularly concerned with the application of SOC to a ‘real world’ physical system: the TCS. We are therefore primarily interested in relating physical features of tropical convection to SOC, and then using this to construct a phenomenological model. The case-study of the seismic system is an excellent example of what this development process could entail and influences the approach that we take in the rest of the project, progressing from: identifying empirical power-law relationships (Chapter 3); to isolating the elements of the dynamics that are SOC (Chapter 4); to formulating a simple cellular automation model (Chapter 5).

Chapter 3

The case for self-organised criticality in the tropical convective system

The purpose of this chapter is to review why the TCS is currently considered as being good candidate for exhibiting self-organised critical behaviour. The main features of convection in the tropics are outlined with particular reference to convective cells, their organisation and the quasi-equilibrium hypothesis. A set of observational studies that all strongly support the conjecture that the TCS is a self-organised critical system are then outlined.

3.1 Convection in the tropics

3.1.1 Meteorological scales

The association of meteorological phenomena with a characteristic spatial and temporal scale is generally successful in the extra-tropics. A prominent example is quasi-geostrophic theory which provides much of the theoretical basis for the understanding of the dynamics of extra-tropical cyclones. In contrast with the extra-tropics, relating the dynamics of the tropical atmosphere to a characteristic scale is largely unsuccessful. This is in large part due to the difficulty in comprehending the moist convective processes, that are the dominant feature of tropical meteorology. It is observed that convective storms can occur at a variety of scales, ranging from isolated thunderstorms that last for less than an hour to systems that extend over hundreds of kilometres and exist for days at a time. Linked to the lack of a characteristic scale is a lack of understanding about the underlying convec-

tive dynamics, with a fully satisfactory description of both the ensemble and individual convective clouds remaining elusive [21].

3.1.2 Convective clouds and organisational structures

Over the tropical ocean convective clouds dominate the structure of the atmosphere and form through the local ascent of buoyant parcels of air. Convective clouds can be classified into two broad categories; shallow cumulus and deep cumulus. Shallow cumulus typically extend from 1000m to 3000m, are of horizontal dimensions of order 100 to 250m and are generally non-precipitating. Deep cumulus clouds extend throughout the depth of the troposphere (approximately 1000m to 8000m), are of horizontal dimensions of order 1km and produce heavy precipitation. Mature deep cumulus clouds are often referred to as cumulonimbus clouds and are frequently associated with thunderstorms. Examples are shown in Figures 3.1(a) and 3.1(b).

There are various mechanisms that can initiate the formation of a convective cloud: advective moisture convergence, radiative cooling, and boundary layer fluxes of moisture and heat all contribute. Collectively these macro-physical processes are referred to as the ‘large-scale forcing’. In response to the large-scale forcing, parcels of air near the surface become unstable and are able to ascend and condense. Sufficiently deep convection produces precipitation. Associated with condensation is the release of latent heat into the troposphere. Convective downdrafts may also form when the precipitation does not reach the surface, but rather evaporates into sub-saturated air. Following a downdraft is the formation of a ‘cold pool’ of boundary layer air that can trigger convection in neighbouring regions of the atmosphere. This has been highlighted in some recent studies as a prominent organisational mechanism for tropical convection [9].

Convective clouds are frequently referred to as convective cells due to the circulatory motion that they induce. Convective cells can be thought of as representing the basic element of a convective system, and when formulating tropical convection as an SOC system, convective cells are thought to represent a DOF. Observations show that tropical convection cells frequently organise into structures that extend far beyond that of individual convective cells. These structures can be linear and are referred to as squall lines or can be non-linear and are referred to as meso-scale convective systems [22].



Figure 3.1: Convective clouds: (a) Shallow cumulus, (b) Mature deep cumulus/cumulonimbus [20]

There are various mechanisms that are known to organise tropical convection, including: wind shear, interaction with large scale waves (such as gravity and Kelvin waves) and the aforementioned cold pool mechanism. Cold pools have a particular significance to SOC as they can be viewed as a short range interaction mechanism between regions of the atmosphere. In contrast with wind-shear and interaction with large scale waves, cold pools are ubiquitous. The SOC model physics developed in Chapter 4 will therefore focus upon the role of the cold pool.

3.1.3 The quasi-equilibrium hypothesis

The Quasi-Equilibrium (QE) hypothesis was introduced by in 1974 by Arakawa and Schubert as a simplifying statistical assumption that could be used to understand the dynamics of a cumulus cloud ensemble [23]. Central to the QE hypothesis is the separation in the timescales between convective adjustment time, (which refers to how long convection takes to adjust itself to changes within the convective ensemble), and variations in large-scale forcing. This was envisaged in the 1974 paper as: ‘*When the timescale of the large-scale forcing is sufficiently larger than the adjustment time, the past history, within the scale of the adjustment time can be represented by the current large-scale forcing. This means that the cumulus ensemble follows a sequence of quasi equilibria with the large scale forcing...we call this the quasi-equilibrium assumption.*’. From an energetics perspective this

simply amounts to convection consuming potential energy at the rate at which it is produced by large scale forcing.

Observational studies broadly support QE. For example, QE predicts that the vertical profiles of temperature and moisture are constrained to be close to a saturated-adiabatic parcel ascent [24], (we explain what is meant by this in Chapter 4). QE also constitutes the framework from which much of the understanding and parameterisation of tropical convection is based upon [25]. It is however a statistical rather than an actual equilibrium, and can only be considered as a leading order approximation: in reality, the tropical atmosphere is a slowly driven non-equilibrium system [26]. QE has the most problems when applied to smaller spatial and temporal scales and many aspects of the theory are still debated. Issues include the time response of a convective cloud ensemble to a change in forcing [27]; and exploring the validity of the time-scale separation in terms of ‘convective memory’ [28].

3.2 Observational studies

3.2.1 European rainfall statistics

The suggestion that SOC is present in the atmosphere was first made as early by Vattay and Harnos (1994) [5]. They showed that the daily average air humidity fluctuations from central Europe over the interval of a year exhibited approximate $1/f$ behaviour. It was speculated that the presence of an atmospheric threshold; saturation, linked this to SOC. This viewpoint was consolidated by Peters and Christensen (2002) [6]. Using rainfall statistics and physical analogues to the seismic system it was argued that the atmosphere has the physical attributes of an SOC system. The results proved central to the credibility of the idea that the atmosphere contains elements of SOC dynamics with an article appearing in *New Scientist* magazine [29].

In order to reach their conclusions, Peters and Christensen analysed a time series from radar measurements with a one minute resolution, that was collected at a site on the German Baltic coast over an 8 month period from January to July 1999. Defining ‘rain events’ as the basic entities of the phenomena, it was demonstrated the number density of rain events per year is inversely proportional to the size of event. This occurs over a

regime spanning at least three orders of magnitude, with the data following a well defined power-law. Furthermore, the number density of ‘rain event duration per year’ was shown to demonstrate a similar power-law relationship when plotted against the event duration. These results are shown in Figures 3.2(a) and 3.2(b) and indicate that no typical size or time scale exists for rain event sizes and durations. An analogy was drawn between the Gutenberg-Richter law (Section 2.3.1, Figure 2.4(a)) and the rainfall data. This led to the suggestion that a mechanism in the atmosphere may have some parallels with the seismic system and be an instance of SOC.

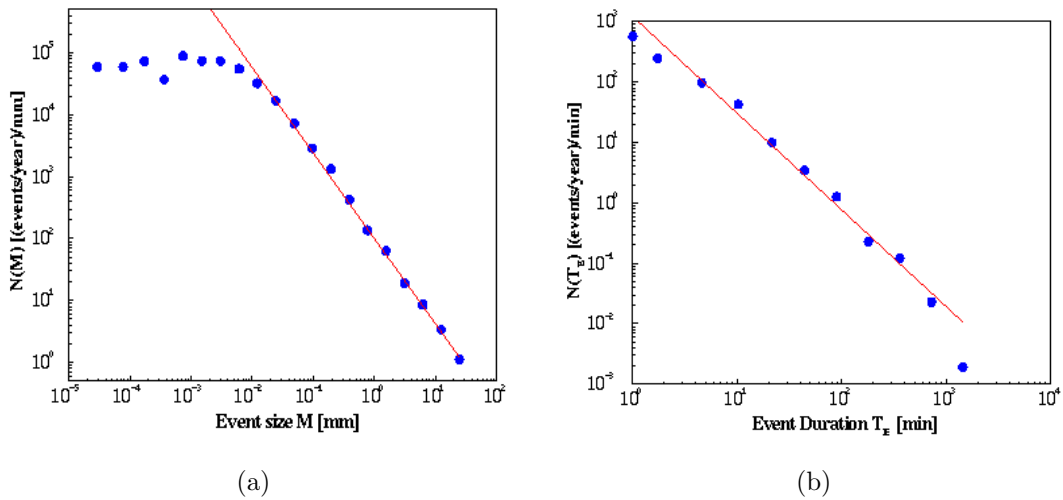


Figure 3.2: Rain event power-law relationships: (a) Number density of rain events against event size, (b) Number density of rain event duration against versus event duration, (both double-logarithmic scale)

3.2.2 $1/f$ behaviour in the Pacific

In recent years, data from the tropics has been used to further support the case that the atmosphere contains elements of SOC. This data has the advantage of isolating convection as the dominant process that is being studied. A detailed analysis of tropical convective variability using Tropical Ocean Global Atmosphere Coupled Ocean Atmosphere Response Experiment (TOGA-COARE) data was carried out by Yano et al. (2003) [7]. Using time series data from 13 sites in the western Pacific, approximate $1/f$ behaviour was found to occur in atmospheric surface variables over an interval from 1 hour to 10 days. Figures

3.3(a) and 3.3(b) show the time series and power spectra that were recorded at one of the observation sites. It is evident that rain events, are correlated to large fluctuations in temperature, moisture mixing ratio and wind speed.

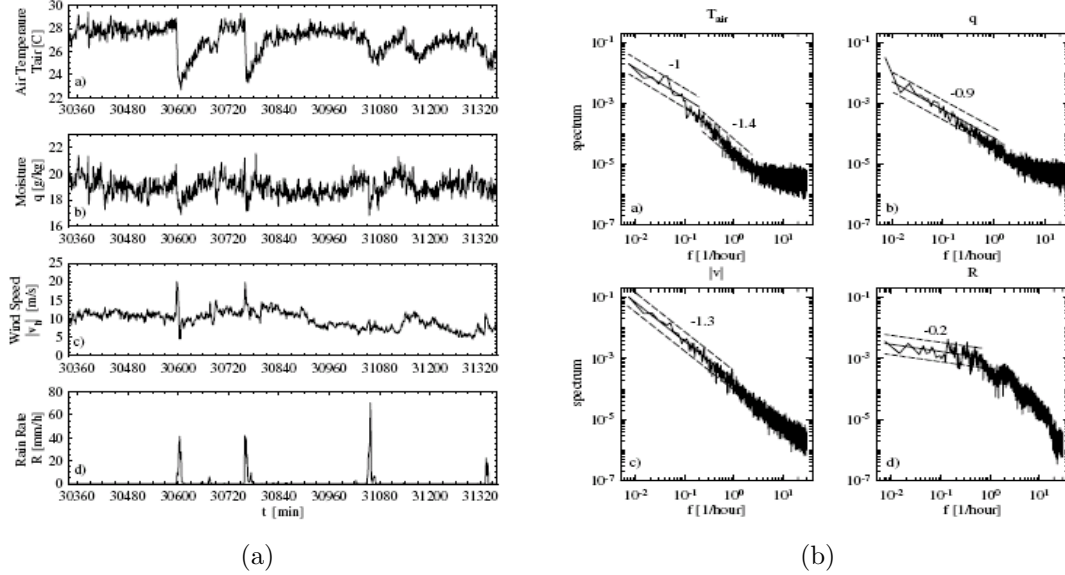


Figure 3.3: TOGA-COARE data from site in mid-Pacific: (a) Time series, (b) Power spectra, for: air temperature T_{air} , moisture mixing ratio q , wind speed $|v|$ and rain rate R , [7]

Specifically, it was established that power-law regimes with $\alpha \in [0.8, 1.4]$ were present for air temperature, moisture mixing ratio and wind speed. This is consistent with the experimental bounds for $1/f$ behaviour outlined in Section 2.1.2. It was suggested that the origin of the $1/f$ behaviour lay in ‘*intermittent pulse-like convective events*’. It was also highlighted that in its current interpretation QE does not predict the scale-free behaviour observed.

3.2.3 Critical phenomena in tropical rain

A more recent study by Peters and Neelin (2006) [8] used tropical rainfall data and predictions from the theory of critical phenomena to approach the search for SOC in the tropical atmosphere from a more direct perspective. The data sets that the study analysed were comprehensive; satellite microwave data from each major global ocean basin over a 5 year period from 2000 to 2005 at a 20 km grid resolution. Analysing the relationship between

vertically integrated water vapour and precipitation, they demonstrated that above a critical value of vertically integrated water vapour precipitation is intense, short-lived, and follows a power-law relationship. Below that critical value, it is weak but more persistent.

This was interpreted as the tropical atmosphere naturally fluctuating about the critical point of a continuous phase transition. As the atmosphere naturally tunes itself to this state, it can be viewed as a system naturally evolving to criticality and thus an instance of SOC. Furthermore, they argued that the balance between large scale forcing and convection postulated in the QE hypothesis could be directly identified with this critical point. It was established that although details, such as the critical value of the vertically integrated water vapour changed, the relationships that linked them to the same form of continuous phase transition did not. An additional expectation from the theory of critical phenomena that they were able to confirm was a peak in the variance of precipitation at this critical water vapour, consolidating the view that a continuous phase transition is present.

This study was the first time that the critical point of an SOC system has been identified from empirical data using the theory of critical phenomena. It can thus be regarded as making both a strong case for SOC in the TCS and for the general development of SOC as a field of research.

3.3 The consequences of Chapter 3 for the project

The empirical studies outlined on this chapter demonstrate a marked progression towards answering the central question; ‘Does SOC occur in the TCS?’. The stages of development can be viewed as:

1. Identifying scale-free behaviour in atmospheric data and making a generalised argument that the atmosphere has the attributes of an SOC system.
2. Isolating the tropical convective system as a likely candidate for SOC and observing $1/f$ behaviour in variables linked to convective events.
3. Directly identifying tropical rainfall data with the predictions of critical phenomena.

By comparison, the seismic system has not been directly related to the critical point of a continuous phase transition. The direct identification of the self-tuning of the tropical atmosphere to a critical point can therefore potentially be regarded as a stronger empirical argument for SOC in the tropical convective system than the seismic system.

However, unlike the seismic system there is yet to be a simple model devised for the TCS that is able to anticipate the criticality that arises. This was highlighted by Peters and Neelin [8] upon identifying tropical convection with critical phenomena; ‘*These findings beg for a simple model of the atmospheric dynamics responsible for the critical behaviour...the physics must conform with recent cloud-resolving model analysis...[and] to the key role of extortory short range interactions*’.

This study seeks to investigate what a cellular automation model of the TCS could look like. It is hoped that the model will be able to reproduce some of the observational evidence outlined in this chapter. The study is highly exploratory and many of the ideas proposed in Chapters 4 and 5 are possible ways of viewing the problem, rather than producing a definitive formulation.

Chapter 4

Model physics

This chapter is concerned with isolating the essential physics from which a cellular automation model of the TCS can be developed. We are primarily interested in identifying and quantifying:

- The nature of the forcing experienced by the TCS.
- The presence of a threshold in the TCS.
- The DOF of the TCS and the interaction that occurs between them.
- The dynamic variable from which the model is to be constructed.

A three-level atmospheric model, (the ‘threshold model’), based upon fundamental stability constraints is developed. This is used to draw conclusions about thresholds and timescales. The nature of a convective cell and the cold pool development process is then used to define the DOF and interaction mechanism. The degree of time-scale separation between convective forcing and relaxation is also investigated and influences the choice of dynamic variable and model formulation.

4.1 Atmospheric physics background

In this section we outline the underlying physics from which the three-level model is constructed.

4.1.1 Atmospheric composition and equation of state

In meteorological applications the Earth's atmosphere is treated as an ideal gas and has the equation of state

$$p = \rho RT, \quad (4.1)$$

where p is the pressure, ρ is the density, R is the molar gas constant and T is the temperature. The gases in the Earth's atmosphere comprise of a mixture of dry air and water vapour and (4.1) can be decomposed into partial equations of state:

$$\begin{aligned} (p - e) &= \rho_d R_d T \\ e &= \rho_v R_v T, \end{aligned}$$

where $(p - e)$ is the partial pressure of dry air and e is the partial pressure of water vapour. The density and gas constant subscripts d and v refer to dry air and water vapour respectively. The water vapor content is quantified by the mixing ratio q

$$\begin{aligned} q &= \frac{\rho_v}{\rho_d} \\ &= \frac{R_d}{R_v} \frac{e}{(p - e)}, \end{aligned}$$

which represents the fraction by mass of water vapour present in the atmosphere. The composition of dry air is approximately fixed, dominated by Nitrogen and Oxygen (75.51% and 23.14% fraction by mass respectively). The amount of water vapour present varies with time and location.

4.1.2 Saturation

The saturation water vapour pressure e^* represents the maximum possible partial water vapour pressure at a given temperature. The Clausius-Clapeyron equation describes this phase equilibrium and is given by

$$\frac{de^*}{dT} = \frac{L_v e^*}{R_v T^2}, \quad (4.2)$$

where L_v is the latent heat of evaporation. Integrating (4.2) for constant L_v gives the following expression for e^*

$$e^* = e_0^* \exp\left(\frac{L_v}{R_v} \left(\frac{1}{T_I} - \frac{1}{T}\right)\right), \quad (4.3)$$

where T_I is a reference temperature. It is clear that e^* is a function of temperature alone. Using (4.3) saturated analogues of other quantities can be defined. For example the saturated mixing ratio q^* is given by

$$q^* = \frac{R_d}{R_v} \frac{e^*}{(p - e^*)}. \quad (4.4)$$

Correspondingly q^* is a well defined function of temperature and pressure. The relative humidity H is defined by

$$H = \frac{e}{e^*},$$

and represents the fraction of water vapour in the atmosphere relative to the saturation level.

4.1.3 Atmospheric stability

Atmospheric stability is assessed by considering the vertical displacement of a parcel of air away from its initial position. The parcel is assumed to not disturb or mix with its environment. Newton's Second Law of Motion for a parcel of density ρ' in an atmosphere of density ρ is

$$f_b \equiv g \left(\frac{\rho - \rho'}{\rho'}\right) = \ddot{z}, \quad (4.5)$$

where f_b is the buoyancy force, g is the gravitational acceleration and z is the vertical coordinate. Using (4.1) we can rewrite (4.5) as

$$f_b \equiv g \left(\frac{T' - T}{T'}\right) = \ddot{z}. \quad (4.6)$$

Equations (4.5) and (4.6) are both forms of the the Archimedean principle, simply stating that parcels of air that are warmer and less dense than their environment experience an upwards buoyancy force. Performing a power series expansion of T and T' about the initial

position $z = 0$, where $T'_0 = T_0$ gives:

$$T(z) = T_0 + \left. \frac{dT}{dz} \right|_{z=0} z + \dots \quad (4.7)$$

$$T'(z) = T'_0 + \left. \frac{dT'}{dz} \right|_{z=0} z + \dots, \quad (4.8)$$

if quadratic and higher order terms are neglected. Substituting (4.8) and (4.7) into (4.6), we obtain

$$\ddot{z} + N^2 z = 0, \quad (4.9)$$

where

$$N^2 = \frac{g}{T_0} \left(\frac{dT}{dz} - \frac{dT'}{dz} \right), \quad (4.10)$$

is the static stability parameter. The derivative terms $\frac{dT}{dz}$ and $\frac{dT'}{dz}$ represent the vertical rate of change of environmental temperature and parcel temperature, (referred to as the environmental and parcel ‘lapse rates’), in the neighbourhood of the initial point. The ordinary differential equation (4.9) is the equation of a simple harmonic oscillator and has solutions of the form

$$z(t) = A \exp(iNt) + B \exp(-iNt),$$

where A and $B \in \mathbb{C}$. The following behaviour can occur dependent upon the sign of N^2 :

$$\begin{aligned} N^2 < 0 & \Rightarrow \text{Unstable atmosphere and unbounded solution} \\ N^2 = 0 & \Rightarrow \text{Neutral atmosphere} \\ N^2 > 0 & \Rightarrow \text{Stable atmosphere and oscillatory solution.} \end{aligned}$$

The physical interpretation is that when the environmental lapse rate is less than the parcel lapse rate, a finite vertical displacement will leave a parcel warmer than its environment and positively buoyant. The converse is true when the environmental lapse rate is greater than the parcel lapse rate.

4.1.4 Static energy and its relation to atmospheric lapse rates

The static energy s , the moist static energy h , and the saturation moist static energy h^* of a parcel of air are defined as:

$$\begin{aligned} s &= c_p T + gz \\ h &= c_p T + gz + L_v q \\ h^* &= c_p T + gz + L_v q^*, \end{aligned}$$

where c_p is the specific heat capacity of air at constant pressure. These are fundamental thermodynamic quantities: s represents the sum of internal and potential energy, h represents the sum of internal, potential and latent energy, and h^* is the saturated analogue of h . All three have dimensions of energy per unit mass. From the definitions above it follows that s is conserved under hydrostatic, adiabatic, unsaturated displacements and h^* is conserved under hydrostatic, adiabatic, saturated displacements. Expressions for the unsaturated-adiabatic and saturated-adiabatic lapse rates, Γ_A and Γ_{SA} can thus be obtained by setting $\frac{ds}{dz} = 0$ and $\frac{dh^*}{dz} = 0$. This gives:

$$\Gamma_A \equiv - \left. \frac{dT}{dz} \right|_A = \frac{g}{c_p} \quad (4.11)$$

$$\Gamma_{SA} \equiv - \left. \frac{dT}{dz} \right|_{SA} = \frac{g}{c_p} + \frac{L}{c_p} \frac{dq^*}{dz}. \quad (4.12)$$

Due to latent heat release $\Gamma_{SA} < \Gamma_A$. Making the substitution of (4.11) and (4.12) for $\frac{dT}{dz}$ in (4.9) leads the following stability regimes:

$$- \frac{dT}{dz} > \Gamma_A \quad \Rightarrow \quad \text{‘Absolute instability’} \quad (4.13)$$

$$\Gamma_{SA} < - \frac{dT}{dz} < \Gamma_A \quad \Rightarrow \quad \text{‘Conditional instability’} \quad (4.14)$$

$$- \frac{dT}{dz} < \Gamma_{SA} \quad \Rightarrow \quad \text{‘Absolute stability’}. \quad (4.15)$$

Absolute instability refers to an atmosphere that is unstable to moist-saturated and dry parcel displacements. Conditional instability refers to an atmosphere that is unstable to moist-saturated but stable to dry parcel displacements. Absolute stability refers to an environment that is stable to both moist-saturated and dry displacements. A non-saturated but moist parcel is equivalent to a dry parcel when assessing stability criteria

4.1.5 Mean tropospheric profiles

An observational study was carried out by Yanai, Esbensen and Chu [30] that investigated the mean tropospheric profiles for s , h and h^* over the Pacific Ocean. The results are shown in Figure 4.1. It was observed that s increases with height, whilst h and h^* have a minimum in the mid troposphere at $p \approx 65\text{kPa}$ and $p \approx 60\text{kPa}$ respectively. We can interpret this in terms of the stability regimes (4.13)-(4.15). A dry parcel is stable throughout the troposphere whilst a moist-saturated parcel is conditionally unstable throughout the lower and mid troposphere and conditionally stable in the mid troposphere. It is also noted that h and h^* are significantly greater than s in the lower troposphere due to the presence of water vapour and relatively high temperature.

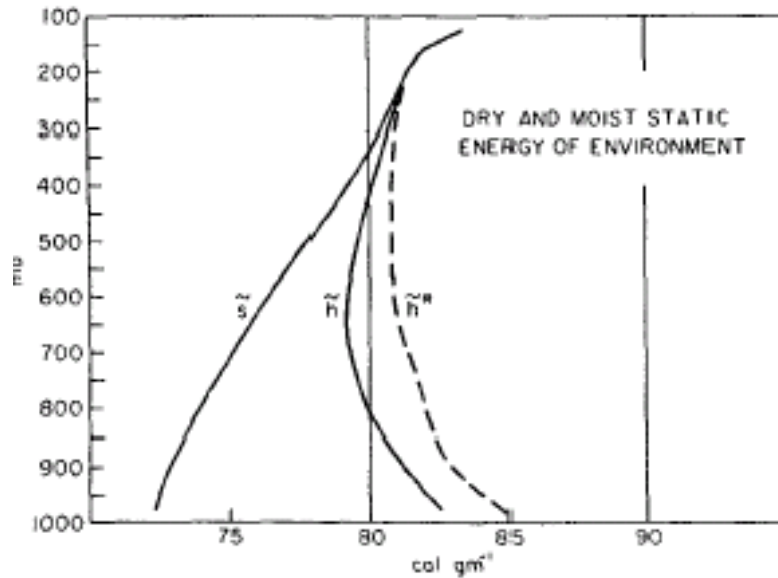


Figure 4.1: Mean tropical tropospheric profiles for s , h and h^* [30]

4.2 Threshold model

In 1968 Arakawa devised an idealised three-level atmospheric model in which he utilised fundamental stability constraints to parameterise a cumulus cloud ensemble in a statistically steady state. The model has proved to be very successful and has been used as a conceptual foundation for the cumulus parameterisation in many global circulation models [31]. SOC systems require the evolution toward a threshold. This is not a feature of the steady-state Arakawa model and it is the aim of this section to revise the Arakawa model to include explicit time dependence and hence to show the corresponding time evolution toward a threshold.

4.2.1 Stability properties of the three level model

The Arakawa model makes the assumption that the thermo-dynamical properties of all clouds are alike and deals with ensemble averaged quantities. This reduces the problem to the vertical dimension with the three levels corresponding to:

1. *The atmospheric boundary layer:* The well mixed sub-cloud, boundary layer at $p \approx 95\text{kPa}$.
2. *The mid troposphere:* The lower layer of shallow cumulus cloud at $p \approx 75\text{kPa}$.
3. *The upper troposphere:* The upper layer of deep cumulus cloud at $p \approx 35\text{kPa}$.

The necessary conditions for deep and shallow convection are given as [31]:

$$h_1 > (h_2^*, h_3^*) > h_2 \quad (4.16)$$

$$h_1 > h_2^*, \quad (4.17)$$

respectively. We are primarily concerned with deep convection that extends from level 1 through to level 3. It follows from (4.16) that:

$$-\frac{T_2 - T_1}{z_2 - z_1} > \frac{g}{c_p} + \frac{L}{c_p} \frac{q_2^* - q_1}{z_2 - z_1} \quad (4.18)$$

$$-\frac{T_3 - T_1}{z_3 - z_1} > \frac{g}{c_p} + \frac{L}{c_p} \frac{q_3^* - q_1}{z_3 - z_1} \quad (4.19)$$

$$-\frac{T_3 - T_2}{z_3 - z_2} < \frac{g}{c_p} + \frac{L}{c_p} \frac{q_3^* - q_2}{z_3 - z_2} \quad (4.20)$$

$$q_2^* > q_2. \quad (4.21)$$

The constraints (4.18),(4.19) and (4.20) can be interpreted as the atmosphere satisfying an intermediate stability condition, $\Gamma_{A/SA}$ that lies in the interval $\Gamma_A > \Gamma_{A/SA} > \Gamma_{SA}$. The physical interpretation is that a parcel ascending from level 1 to levels 2 and 3 becomes saturated at an intermediate point upon ascent. This analysis is in direct correspondence with Emanuel’s interpretation of the conditions for instability: ‘*The degree of instability is approximately measured by the difference between the moist static energy of the sub-cloud layer air and the saturation moist static energy of the air above*’ [24]. For deep convection to occur, level 1 is ‘ $\Gamma_{A/SA}$ unstable’ with respect to levels 2 and 3, whilst level 2 is ‘ $\Gamma_{A/SA}$ stable’ with respect to level 3. The final constraint (4.21) signifies that the atmosphere is unsaturated in the mid troposphere.

4.2.2 Forcing

It is a feature of SOC systems that they are gradually driven until reaching a dynamical threshold point. We propose that in the TCS this could correspond to long-wave radiative cooling and boundary layer forcing through surface fluxes. These are ubiquitous and broadly homogenous forcing terms, and can be considered as leading order effects that are essential to consider in our model. Advective moisture convergence is neglected as it is a local effect, rather than representing a drive for the full TCS.

In the tropics, the longwave radiative cooling rate of the Earth’s atmosphere $-F_r$ is of order $-2 \times 10^{-2} \text{Js}^{-1}$, which corresponds to roughly -2Kday^{-1} . This extends throughout the depth of the troposphere and varies dependent upon the emissivity properties of different atmospheric layers. Boundary layer forcing of s and q , F_s and F_q , is parameterised by the bulk aerodynamic formulae:

$$F_s = \frac{g\rho_G C_D |\mathbf{v}|}{\Delta p_B} (s_G - s_1) \quad (4.22)$$

$$F_q = \frac{g\rho_G C_D |\mathbf{v}|}{\Delta p_B} (q_G^* - q_1), \quad (4.23)$$

where the subscript G refers to the ground level, C_D is the dimensionless drag co-efficient, $\Delta p_B = p_G - p_1$ is the difference between the pressure at the ground and at level 1 (B notates ‘boundary’) and $|\mathbf{v}|$ is the wind speed. Expressions (4.22) and (4.23) assume mean values

of the corresponding variables and that turbulent fluxes are proportional to the vertical gradient. Typical parameter values are $C_D \approx 0.001$ and $|\mathbf{v}| \approx 5\text{ms}^{-1}$ when $\Delta p_B \approx 5\text{kPa}$ [24]. The resultant effect of long-wave radiative cooling and boundary layer forcing is that a build up of energy occurs in the atmospheric boundary layer. Once the instability threshold is met, this can be redistributed by convective motion and latent heat release in the rest of the troposphere.

4.2.3 Level budget equations and solutions

The Arakawa model is based around budget equations for s and q . The 3 levels are coupled through the action of convection and a steady state solution is obtained that considers forcing in equilibrium with convection. We will revise this by decoupling the layers, thereby considering the build-up towards convection rather than the steady-state action of the convection.

In the absence of advection and level coupling the budget equations for s and q are:

$$\begin{aligned}\frac{\partial s_1}{\partial t} &= -F_{r1} + \frac{g\rho_G C_D |\mathbf{v}|}{\Delta p_B} (s_G - s_1) \\ \frac{\partial s_2}{\partial t} &= -F_{r2} \\ \frac{\partial s_3}{\partial t} &= -F_{r3},\end{aligned}\tag{4.24}$$

$$\begin{aligned}\frac{\partial q_1}{\partial t} &= \frac{g\rho_G C_D |\mathbf{v}|}{\Delta p_B} (q_G^* - q_1) \\ \frac{\partial q_2}{\partial t} &= 0 \\ \frac{\partial q_3}{\partial t} &= 0,\end{aligned}\tag{4.25}$$

which are a set of first order, evolutionary partial differential equations. Assuming constant $-F_r$ at each level, analytical solutions for levels 2 and 3 are trivial. In general, an analytical solution of the level 1 equations does not exist. However for fixed s_G and q_G^* an analytical solution can be obtained by using the integrating factor method. Physically this approximation corresponds to the surface being held at a fixed temperature and pressure (as the functional dependence is: $s_G(T)$ and $q_G^*(T, p)$). This is a good approximation to

make over a tropical ocean where the water temperature remains approximately fixed over the diurnal cycle and pressure fluctuations are small. The solutions for the equation sets (4.24) and (4.25) are then:

$$\begin{aligned}
 s_1 &= \left(s_G - \frac{F_{r1} \Delta p_B}{g \rho_G C_D |\mathbf{v}|} \right) + \left[s_{1I} - \left(s_G - \frac{F_{r1} \Delta p_B}{g \rho_G C_D |\mathbf{v}|} \right) \right] \exp \left[\left(\frac{-g \rho_G C_D |\mathbf{v}|}{\Delta p_B} \right) t \right] \\
 s_2 &= -F_{r2} t + s_{2I} \\
 s_3 &= -F_{r3} t + s_{3I}
 \end{aligned} \tag{4.26}$$

$$\begin{aligned}
 q_1 &= q_G^* + (q_{1I} - q_G^*) \exp \left[\left(\frac{-g \rho_G C_D |\mathbf{v}|}{\Delta p_B} \right) t \right] \\
 q_2 &= q_{2I} \\
 q_3 &= q_{3I},
 \end{aligned} \tag{4.27}$$

where the subscript I notates the initial data. It is noted that these constants of integration have functional dependence upon a vertical coordinate (either p or z), which is representative of our initial arbitrary choice of level heights. Using the level solutions for $s(t)$ and $q(t)$, (4.26) and (4.27), it is straightforward to obtain the evolution of $h(t)$. The evolution of $h^*(t)$ follows from (4.24) and (4.4).

4.2.4 Evolution toward a threshold

We are interested in estimating the time period, τ_C , that it takes for a ‘relaxed’ region of the atmosphere to reach the deep convective instability threshold (4.16). Data from an observational study by Betts [32] is used to prescribe initial conditions. The data originates from a set of vertical sounding profiles of s and q taken in the aftermath of a convective storm at $8^\circ N$ in the mid-Atlantic Ocean. The initial conditions are shown in Table 4.1. As radiative forcing data was unavailable from this study approximate values for a tropical atmosphere from [30] were used for the final column.

Figure 4.2 shows the evolution of h and h^* over 24 hours. We observe that h_1 increases due to the forcing terms F_s and F_q . All other terms decay in accordance with longwave radiative cooling. Utilising the stability criteria, (4.16) and (4.17) we observe that $h_1 > h_2^*$ at $t \approx 6$ hrs and $h_1 > h_3^*$ at $t \approx 12.5$ hrs. The criteria $h_3^* > h_2$ and $q_2^* > q_2$ are met for all times. This corresponds to a shallow convective event occurring at 6 hours and a deep

convective event occurring at 12.5 hours. This is thought to represent a lower bound as the shallow convection would alter the equation set, introducing a coupling between layers 1 and 2. Observations from [7] consolidate this view where typically, one major deep convective event is observed in an 18 hour time period. We further discuss the implication of this convective timescale, τ_C , in Section 4.4.

Quantity	p	z	T	s	Lq	h	$-F_r$
Units	kPa	km	K	10^5 Jkg^{-1}	10^4 Jkg^{-1}	10^5 Jkg^{-1}	10^{-2} Js^{-1}
G	100	0	296	2.96	-	-	-
1	95	0.710	295	3.02	3.50	3.37	-2.4
2	75	2.550	285	3.10	2.20	3.31	-1.2
3	35	8.780	250	3.36	0.40	3.40	-1.8

Table 4.1: Initial conditions (adapted from diagrams in [32] and [30])

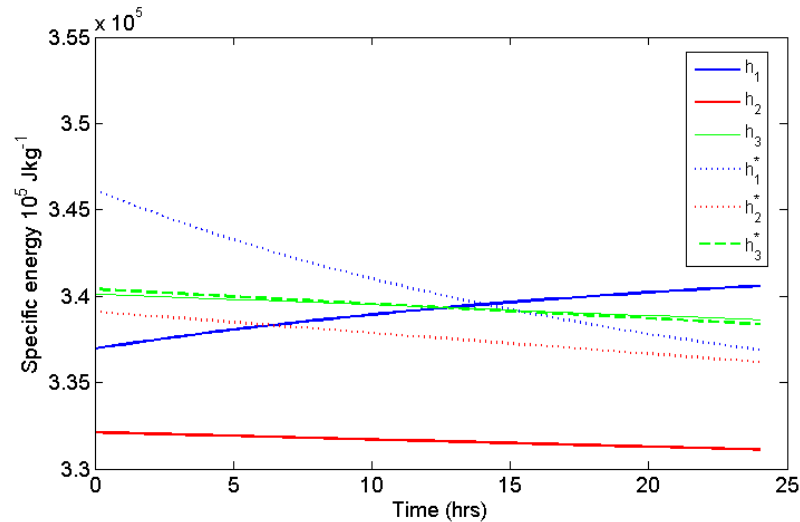


Figure 4.2: Evolution of h and h^* over the interval $t \in [0, 24\text{hrs}]$.

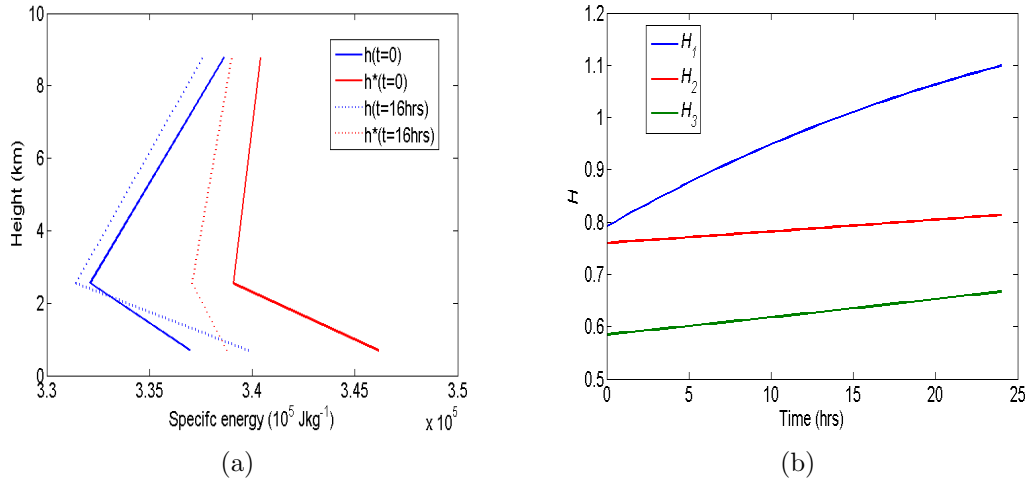


Figure 4.3: (a) Vertical profiles of h and h^* at $t = 0$ and $t = 16$ hrs, (b) Evolution of H over the interval $t \in [0, 24\text{hrs}]$

Figure 4.3(a) shows vertical profiles for h and h^* , based upon the threshold model. The crossing of h_1 and h_3^* by 16 hours indicates that the atmosphere is unstable to deep convection through (4.16). This enables us to think about the TCS in slightly different way than the statistically steady state of the QE hypothesis. By comparing 4.3(a) with [30], various convectively stable states can be considered as a fluctuation about a mean tropospheric profile for h and h^* . A build up of moist static energy in the atmospheric boundary layer until (4.16) and (4.17) are met is then followed by a convective event that ‘resets’ the atmospheric variables. The presence of the convective threshold ensures that the TCS resembles an equilibrium system.

Figure (4.3(b)) shows the evolution of H (defined in Section 4.1.2) over a 24 hour interval. Level 1 becomes saturated at approximately the same time that the atmosphere becomes unstable to deep convection. In reality, this is likely to occur at a later time due to the moisture transport that is associated with shallow convection. We can therefore conclude that the threshold model behaves sensibly with respect to saturation considerations.

4.3 Relaxation and interaction mechanisms

Convective cells can be considered as the basic elements of a convective system. These are used to represent the DOF in the cellular automation model that is formulated in Chapter 5. Firstly, this section outlines the lifecycle of a convective cell and the associated cold pool that develops. This is then used to explore what the relaxation and interaction mechanisms in the cellular automation model could correspond to.

4.3.1 The life cycle of a convective cell and its relation to cold pool formation

A schematic diagram of the physical process that are related to cold pool formation is shown in Figure 4.4. This cold pool exists in the atmospheric boundary layer, perturbing T_1 and q_1 in regions neighbouring a convection cell. We are interested in identifying how these processes govern the h_1 budget of the boundary layer, as this can be related to the threshold model stability constraints. Three distinct stages of development are identified:

- **A:** Deep convection initiates and associated precipitation occurs. Subsequently boundary layer air is cooled and moistened by the evaporation of precipitation.
- **B:** The evaporation of precipitation into sub-saturated air results in the formation of negatively buoyant regions of air in the sub-cloud layer. A downdraft forms, resulting in the introduction of cold, dry air into the lower boundary layer and the advection of the initial moist air towards the edges of the newly formed cold pool (the ‘gust-front’). The net result is a positive perturbation to q_1 at the edge of the pool and a negative perturbation to q_1 in the centre. The perturbation to T_1 is negative throughout the region, peaking in the centre.
- **C:** The convective cell dissipates and the temperature recovers in the central region. A further negative perturbation to q_1 occurs throughout the region due to dry air being entrained from above into the boundary layer. The gust-front region mixes with the cold pool, dissipating the positive perturbation to q_1 at the boundary.

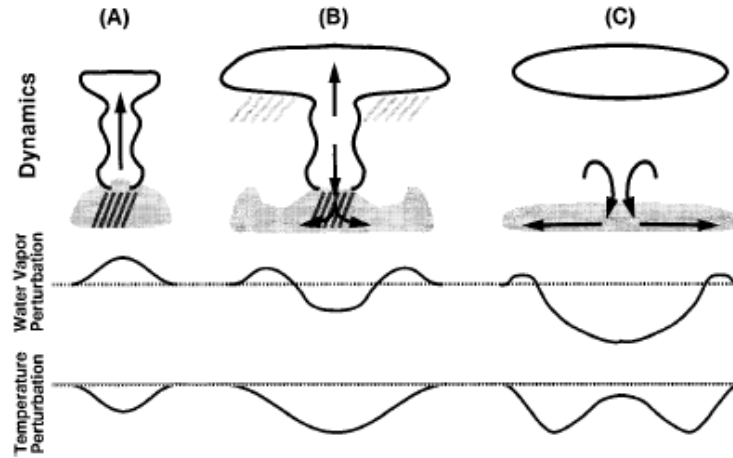


Figure 4.4: Schematic diagram of cold pool development and the associated T_1 and q_1 perturbations in the boundary layer [9]

The thermodynamical role of cold pools as an organisational mechanism for tropical convection was investigated by Tompkins [9] using a high resolution cloud resolving model. Leading order thermodynamic mechanisms were isolated by investigating simulations of an idealised case with constant sea surface temperature and no wind shear. It was established that the gust-front was responsible for triggering convection in neighbouring regions to the original convective cell. The contrasts with previous theories where it was assumed that dynamical mechanisms (such as wind shear), play a dominant role in the organisation of tropical convection. We therefore aim to incorporate this leading order thermodynamic interaction into our SOC model. (Note that the cold pool mechanism is considered a ‘thermodynamic interaction’ from an atmospheric physics perspective, but as a ‘dynamic interaction’ from a complexity/SOC viewpoint).

4.3.2 Consequences of the cold pool for the model

The data given in [9] for T_1 and q_1 is assessed with respect to a mean background state. It is argued in [9] that the moisture perturbation at the gust-front is the dominant mechanism for the onset of convection. It is hoped that by using the moisture perturbation values given in [9], an approximate picture of the h_1 budget can be obtained. This can then be used to give a reasonable estimate of the effects of the cold pool on the potential for convective initiation in the region surrounding the convection cell.

Moisture perturbations from the mean state for the gust-front and pool centre are $q'_{1gust} = 0.25 \text{ gkg}^{-1}$ and $q'_{1centre} = -1.30 \text{ gkg}^{-1}$ respectively. This corresponds to h_1 perturbations of $h'_{1gust} = 625 \text{ Jkg}^{-1}$ and $h'_{1centre} = -3250 \text{ Jkg}^{-1}$. The overall picture is therefore a major relaxation occurring at the convection site and a minor perturbation occurring in a neighbouring region. An approximate comparison can be made to the initial conditions used in the threshold model in Section 4.2.4. The ‘relaxation’ amount $h'_{1centre}$ is roughly analogous to the difference in h_1 between a relaxed and convectively unstable atmosphere in the threshold model, and at -3250 Jkg^{-1} and -2700 Jkg^{-1} are in close agreement. The value of h'_{1gust} is approximately a quarter of the amount required to drive a relaxed atmosphere to the threshold. It is this perturbation that can cause the onset of convection in regions surrounding a convective cell.

The mean lifetime of the cold pool development process, was established to be 2.5 hours. The gust-front moisture perturbation exists from approximately 30 minutes after the original convective cell forms, and is located at the outer extremity of the cold pool which has a mean radius of 8.6km. The majority of the relaxation at the point of convection occurs during the initial 30 minutes, representing the lifecycle of the cloud itself. Due to the intricacy of the cool-pool mechanism it is hard to describe by a single timescale as was possible for convective instability. Nevertheless, in order to make comparisons and assess the timescale separation between convection and relaxation, the cold-pool ‘relaxation/interaction’ timescale τ_R is introduced where approximately $\tau_R \in [30\text{mins}, 2.5\text{hrs}]$.

4.4 Summary and development of model physics

4.4.1 Dynamical features of the TCS

This chapter has demonstrated that the convective system has many of the features that are considered as necessary for SOC to occur. The challenge is now to integrate these ideas into a consistent and simple framework from which a cellular automation algorithm can be developed. To further clarify the dynamical features that we have isolated as begin relevant to SOC, a comparison with the granular and seismic systems is made in Table 4.2.

System	Granular pile	Seismic	Convective
Degrees of freedom	Granular column	Spring-block	Convection cell
Energy storage	Gravitational potential energy	Tension	Boundary layer moist static energy
Threshold	Slope angle	Friction	Deep convective instability constraint
Release of energy	Avalanche	Earthquake	Convective event
Interaction mechanism	Transfer of grains	Momentum transfer between blocks	Cold pool gust-front perturbation

Table 4.2: A comparison between the dynamical features of the granular, seismic and convective systems

4.4.2 Time-scales in the TCS

In Section 4.2.4 the threshold model estimated τ_C to be in the interval $\tau_C \in [12.5\text{hrs}, 18\text{hrs}]$. An approximate check of this can be made by comparing with observational data. Figure 4.5 is an image showing the global annual mean deep convective cloud cover percentage [33]. Tropical ocean regions typically have 4-9% of deep convective cloud cover. By a simple scaling argument and assuming a convective cloud life span of an hour, this would correspond to approximately $\tau_C \in [11\text{hrs}, 25\text{hrs}]$, in general agreement with the findings of Section 4.2.4. τ_C arose from considering radiative and boundary layer forcing alone - it is representative of the time period that it takes convection to occur in absence of any interaction mechanism. As much of this deep convective cloud is likely to have arise from a mechanism other than a threshold being reached in isolation, (such as the cold pool mechanism), it is thought reasonable to extend the upper bound on τ_C to 48 hours.

Section 4.3.2 estimated the relaxation/interaction timescale τ_R to be in the approximate interval $\tau_R \in [30\text{mins}, 2.5\text{hrs}]$. From τ_C and τ_R we can estimate the degree of time-scale separation between the drive/energy storage phase and the sudden burst/release of energy in the TCS. This time-scale separation corresponds to the ratio τ_R/τ_C , which from the bounds upon τ_C and τ_R can be estimated as being in the interval $\tau_R/\tau_C \in [\frac{1}{96}, \frac{1}{5}]$. The analogous time-scale separation in the granular and seismic systems is more pronounced, with the time period of the ‘relaxation’ of avalanches and earthquakes being incrementally small compared with the time period associated with adding grains and driving plates. Relaxation and interaction are subsequently implemented as being instantaneous effects

in the granular and seismic cellular automation models. This would be non-physical for the TCS, and our model will endeavour to take this into account.

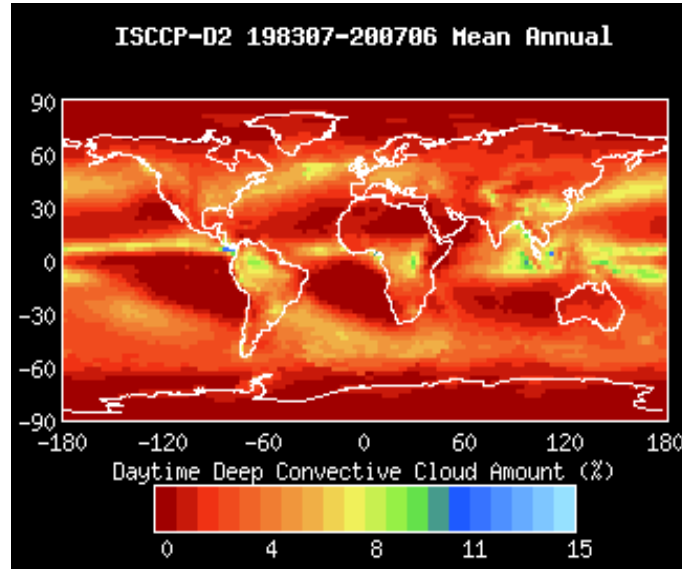


Figure 4.5: Image of mean annual deep convective cloud cover percentage [33]

4.4.3 Steps toward a cellular automation model of the TCS

In the OFC earthquake model (outlined in Section 2.3), the cellular automation algorithm follows directly from equations of motion for the spring-blocks and is defined in terms of a single dynamic variable for each lattice point, F_{ij} . There is no simple analogue of this process for the TCS and choosing the dynamic variable for the cellular automation is an open question. Here, we outline how a cellular automation algorithm for the TCS can be formulated in terms of a local time variable for each DOF:

- As a simplification, it is assumed that (in absence of cold pool interaction) each DOF follows the same temporal evolution during the driving stage as the threshold model.
- In general, each DOF is at a different stage of temporal evolution and a local variable the ‘age of site’, A_{ij} is subscribed to each point. As T , q and h are functions of t in the threshold model level equations, they can now be viewed as functions of A_{ij} .

- A convective event occurs at a point when the condition for deep penetrating convection is met at a point. (Shallow convection is neglected). Once convection occurs a perturbation to h_1 is applied to neighbouring convection points. Equivalently this can be viewed as enabling neighbouring sites that have reached a sufficiently large age to convect. Interaction between DOF therefore also be formulated in terms of A_{ij} .

The model physics that we have explored has not explicitly considered how to formulate the intensity of an event (and the subsequent relaxation), that occurs at a site. Nevertheless, we have argued that the threshold model and cold pool data have relaxation values that are consistent. We therefore hope to explore a set of possible relaxation mechanisms, that are approximate parameterisations rather than physically direct representations.

Chapter 5

A cellular automation model of the tropical convective system

In this chapter we develop a cellular automation model of the TCS. This is based upon an existing model algorithm developed by Sinha-Ray and Jensen [34]. We use the model physics discussed in Chapter 4 to adapt, extend and re-interpret this model in terms of the physics of convection. Specifically, our contribution is to:

- Investigate the region of parameter space, not previously explored, that is relevant to the TCS.
- In this region, obtain diagnostics that indicate if the system is behaving as critical.
- Conduct an investigation that explores various parameterisations of convective relaxation that have significance for the TCS.
- Investigate how the size of the lattice influences the simulation results.

5.1 The development of the model

This section proceeds through outlining the model terminology, followed by the cellular automation algorithm and then finally discussing the relevance of the algorithm to the model physics.

5.1.1 Model overview and terminology

The model is defined by 2-dimensional cellular automation process on an $L \times L$ lattice indexed by (i,j) . A dynamic variable, the age A_{ij} is assigned to each site and is stored in a matrix $\underline{\mathbf{A}}$. Sites are classified into three types: *suppressed*, *quiescent* and *active*. A second matrix, $\underline{\mathbf{B}}$ is used to record the status of a site. Quiescent sites can become active through two mechanisms:

- *Inter-convection*: Through a nearest neighbour being active.
- *Auto-convection*: Through the site crossing a threshold age A_C independent of nearest neighbour interactions.

Suppressed sites correspond to $A_{ij} < A_P$ where A_P is the lower-bound for inter-convection to occur and quiescent sites correspond to $A_P \leq A_{ij} < A_C$. Equivalently, (in terms of status); $B_{ij} \equiv \textit{suppressed}$ and $B_{ij} \equiv \textit{quiescent}$. Active sites are defined by $B_{ij} \equiv \textit{active}$ alone. The reason for this is because active sites are reset instantaneously in the cellular automation algorithm and have a non-unique age range. The reset parameter is given by A_R .

5.1.2 The cellular automation algorithm

The steps of the cellular automation process are as follows:

0. *Initialisation*: Random, uniformly distributed initial ages $A_{ij} \in [(A_P - A_R), A_C)$ are assigned to each site.

1. *Auto-convection*: Sites are tested for auto-convection threshold. If this is met, sites are relaxed and classified as being active.

$$\begin{aligned} \text{If } A_{ij} > A_C &\Rightarrow A_{ij} \longrightarrow A_{ij} - A_R \\ &\Rightarrow B_{ij} \equiv \textit{active} \end{aligned}$$

2. *Drive*: All sites are incremented by an age interval δA .

$$A_{ij} \longrightarrow A_{ij} + \delta A, \forall ij$$

3. *Inter-convection*: Nearest neighbours are tested for inter-convection threshold. If this is met, nearest neighbours are relaxed and classified as being active. Previously active sites are suppressed.

$$\begin{aligned} \text{If } B_{ij} \equiv \textit{active} \text{ and } A_{i\pm 1j} > A_P, &\Rightarrow A_{i\pm 1j} \longrightarrow A_{i\pm 1j} - A_R \\ &\Rightarrow B_{ij} \equiv \textit{suppressed} \\ &\Rightarrow B_{i\pm 1j} \equiv \textit{active} \end{aligned}$$

$$\begin{aligned} \text{If } B_{ij} \equiv \textit{active} \text{ and } A_{ij\pm 1} > A_P, &\Rightarrow A_{ij\pm 1} \longrightarrow A_{ij\pm 1} - A_R \\ &\Rightarrow B_{ij} \equiv \textit{suppressed} \\ &\Rightarrow B_{ij\pm 1} \equiv \textit{active} \end{aligned}$$

The re-assignment of B_{ij} , $B_{i\pm 1j}$ $B_{ij\pm 1}$ comes after all sites have been tested for the inter-convection condition and reset. This ensures that ‘double-counting’ does not occur.

4. *Return to step 1*

Periodic boundary conditions are assumed: $A_{i1} = A_{iL} \forall i$ and $A_{1j} = A_{Lj} \forall j$. The model is deterministic except for the initialisation of random ages. An overview of the simulation code is given in Appendix A.1.

The cellular automation algorithm over 9 iteration steps is shown in Figure 5.1. This is at an arbitrary stage of evolution, rather beginning with the initial conditions. Opposite domain boundaries are duplicates in accordance with the periodic boundary conditions. An initial distribution of suppressed (dark blue), quiescent (dark red) and active (light green) sites is shown in the first slide. Activity spreads through inter-convection between neighbouring quiescent sites. An active site becomes a suppressed site in the next iteration step. The fifth slide shows a quiescent site becoming active through auto-convection. In turn, this triggers a separate sequence of inter-convection. The eighth slide shows a suppressed site becoming quiescent.

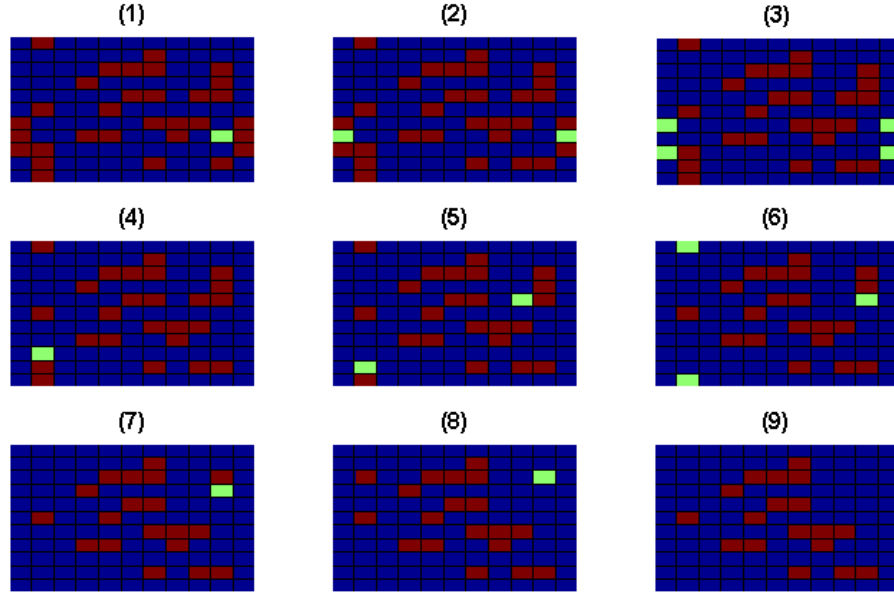


Figure 5.1: The tropical convection cellular automation iteration process with periodic boundary conditions over 9 iteration steps

5.1.3 Relation to model physics

A_C represents the time interval that it takes a site to reach the threshold age in the absence of nearest neighbour interaction, and is normalised to 1. Sites can have an age in the interval $A_{ij} \in [(A_P - A_R), A_C)$. This lower bound arises through considering relaxation at a site with the smallest age that can inter-convect.

The drive increment of the model δA separates the auto-convective and inter-convective steps. δA can therefore be viewed as representing the time interval between a convective event and the moisture perturbation arising at a neighbouring point and has a similarity to τ_R . A_P is related to the strength of the moisture perturbation, with greater values of A_P corresponding to a smaller moisture perturbation being applied at a neighbouring region. The time-scale ratio τ_R/τ_C approximately corresponds to $\delta A/A_C$. This is not a direct relationship as it depends upon the choice of A_R , and the fact that auto-convecting and inter-convecting cells are reset to different ages. Time-scale separation occurs for $\delta A/A_C \ll 1$, corresponding to $\tau_R/\tau_C \ll 1$.

Relaxation at a site occurs instantaneously in the model. Although not physically correct, this is justifiable, as in the cold-pool development process the relaxation in a convecting location is almost complete before a moisture perturbation is established at a neighbouring region. This consolidates the view that τ_R is best representative of the interaction time-scale, rather than relaxation at a site. The initial relaxation mechanism; $A_{ij} \rightarrow A_{ij} - A_R$, means that auto-convecting sites are reset to a greater age than inter-convecting sites. This parameterisation can be viewed as the ‘convective reset value being highly sensitive to the conditions at initiation’, rather than anything directly physical. Other relaxation mechanisms will be considered in Section 5.4.

The periodic boundary conditions correspond to a homogenous, infinite domain. Every lattice point is considered equal. In reality tropical convection is primarily confined over tropical oceans. Physical boundaries exist over continents and toward higher latitudes. Nevertheless as we are concerned with isolating a spatial regime where SOC dynamics may be present, periodic boundary conditions are as physically justifiable as any other simple choice. The distance between lattice points is representative of the mean cold pool radius, established to be 8.6 km in Section 4.4.2.

5.2 Model testing

5.2.1 Relationship to the forest-fire models

In this section we compare our simulation results to the work of Sinha-Ray and Jensen [34] and Drossel and Schwabel [35]. This is done: to check that the model code has been implemented correctly; to explore the model diagnostics of scale-invariant phenomena; and to make an attempt at defining what the critical state of the model refers to. The original form of the model is referred to as the ‘Deterministic Forest Fire model’, (from herein the DFF model) [34]. In the DFF model ‘fire sites’ are active sites, ‘tree sites’ are quiescent sites and ‘empty sites’ are suppressed sites. Trees ignite through either a nearest neighbour being on fire, or by reaching a threshold age. This is directly analogous to inter-convection and auto-convection. The ordering of the DFF algorithm is not made explicit and therefore may be different from our implementation. For clarity we will continue to discuss the models in terms of the convection model terminology presented in Section 5.1.1.

The DFF model was originally proposed as a bridge between deterministic SOC models such as the OFC earthquake model outlined in Chapter 2, and the original ‘Stochastic Forest Fire model’ (from herein the SFF model) [35] - there was no direct physical application in mind. A mean-field theory exists for the SFF, and gives the necessary conditions for the model to evolve toward a critical state [36]. Because the DFF model yields similar results to the SFF model it was suggested that the mean-field theory developed for the SFF model could potentially have significance for the DFF model [34]. We will investigate this idea further in Section 5.2.2

5.2.2 Is the model critical?

In the SFF model the deterministic site evolution through intervals of δA , is replaced by two ‘stochastic evolution mechanisms’:

- a : The probability that a quiescent site becomes active through auto-convection.
- b : The probability that a suppressed site becomes quiescent.

Each quiescent site is tested for becoming active and each suppressed site is tested for becoming quiescent with each iteration step. Inter-convection is defined the same way as before, with activity able to progress between connected quiescent sites [35].

The mean-field theory is defined in the continuum limit of the discrete iteration process and makes the further approximation that inter-convection occurs through only one nearest neighbour at a time [36]. The system is found to be critical in the double limit:

$$b \longrightarrow 0 \tag{5.1}$$

$$a/b \longrightarrow 0. \tag{5.2}$$

A direct relationship between the DFF model and the parameters a and b does not exist. This means that questions arise such as the necessary relationship between A_C , A_P , A_R and δA for the model to be critical, and the number of iterations that are required for the model to approach a critical state. We propose that a working definition of the critical limit for the DFF model, can be obtained by numerically evaluating (5.1) and (5.2).

Figures 5.2(a) and 5.2(b) show the evolution of a/b from two sets of parameter values that are similar to those used by [34], (with the exception of a smaller lattice size index of $L = 50$). The different colours correspond to different sets of initial conditions. It is clear that, independent of initial conditions, both parameter sets evolve toward an approximately steady value of a/b . These correspond to $a/b \approx 0.08$ for $\delta A/A_C = 10^{-3}$ and $a/b \approx 7 \times 10^{-3}$ for $\delta A/A_C = 10^{-4}$. This is what is anticipated by the mean-field theory: the evolution toward a steady state for a and b in accordance with (5.1) and (5.2) [36].

The evolution of b was also investigated. It was established to follow a similar evolution to a/b , with $b \approx 10^{-3}$ and $b \approx 10^{-4}$ for $\delta A/A_C = 10^{-3}$ and $\delta A/A_C = 10^{-4}$ at the steady state respectively. Graphical output is similar in form to Figure 5.2. It is, perhaps, surprising how quickly the steady state is reached for a/b and b ; in approximately $A_C/\delta A$ iterations. Future simulations will take this into account before outputting data. It is hoped that b and a/b will serve as a working indicator of a critical steady state in other simulations.

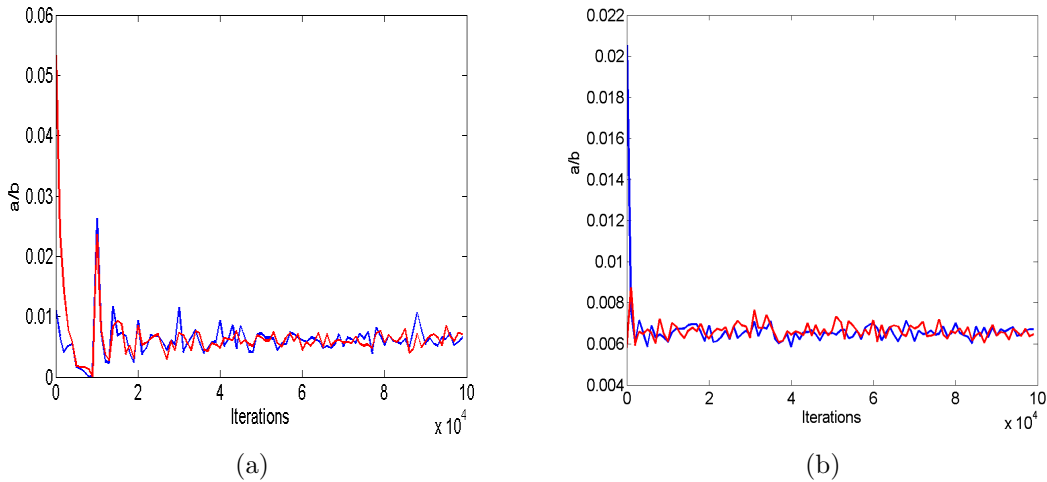


Figure 5.2: Evolution of a/b for: $A_C = 1.0$, $A_R = 1.0$, $A_P = 0.0$: (a) $\delta A = 10^{-3}$, (b) $\delta A = 10^{-4}$

5.2.3 Scale-invariant diagnostics

To be considered as self-organised critical, a model must produce evidence of spatial and temporal power laws. The SFF and DFF models propose that the power spectra of the time series of the number of quiescent sites on the lattice $n_Q(t)$, can be used as a temporal power-law diagnostic. This is obtained by taking the Fourier transform, (2.3), of n_Q , thus obtaining the power spectrum S_Q . The probability of a cluster of quiescent sites P_Q being of size r_Q is proposed as a diagnostic of a spatial fractal. Scaling regimes where $S_Q \propto f_Q^{-\alpha}$ and $P_Q \propto r_Q^{-\beta}$ will therefore correspond to power-law relationships.

There is a clear meteorological interpretation for r_Q . This is because upon one site becoming active all connected quiescent sites are part of the same sequence of inter-convection. They can therefore be considered as part of the same ‘storm’, and the relationship between r_Q and P_Q can be viewed as being related to convective event size distributions. It is anticipated that this diagnostic will become less useful when two originally unconnected clusters of quiescent sites become connected. This is more apparent for larger values of $\delta A/A_C$, and arises due to the finite nature of τ_R .

There is no such obvious meteorological interpretation for the relationship between f_Q and S_Q . However, it does provide a good indication of the behaviour of relative distribution of sites on the lattice.

5.2.4 Comparison between simulation results

A grid size of $L = 50$ corresponding to 2500 sites, and a parameter set similar to that used by Sinha-Ray and Jensen [34] is for comparison purposes. The graphical output format corresponds to:

- (a) Timeseries of n_Q (for the steady state)
- (b) Double logarithmic plot of S_Q against f_Q
- (c) Double logarithmic plot of P_Q against r_Q
- (d) Example of lattice structure,

and will be used throughout this chapter. Data sampling methods are outlined in more detail in Appendix A.2. The structure plots are for an arbitrary iteration step and show

the distribution of suppressed, quiescent and active sites. They are included to provide a qualitative insight toward the organisational structures that arise.

The results are shown in Figure 5.3. A power-law relationship is observed between S_Q and f_Q with exponent $\alpha \approx 2.4$ over approximately two orders of magnitude. This is in agreement with the result of Sinha-ray and Jensen [34], shown in Figure 5.4(a). This does not correspond to $1/f$ behaviour, and is closer to a correlated Brownian signal as is suggested by the time-series for n_Q . A power-law relationship is also observed between P_Q and r_Q with exponent $\beta \approx 1.9$, again over approximately 2.5-3 orders of magnitude. This is again in close agreement with the result of Sinha-ray and Jensen [34] shown in Figure 5.4(b). We can therefore conclude that our model and sampling methods are implemented correctly.

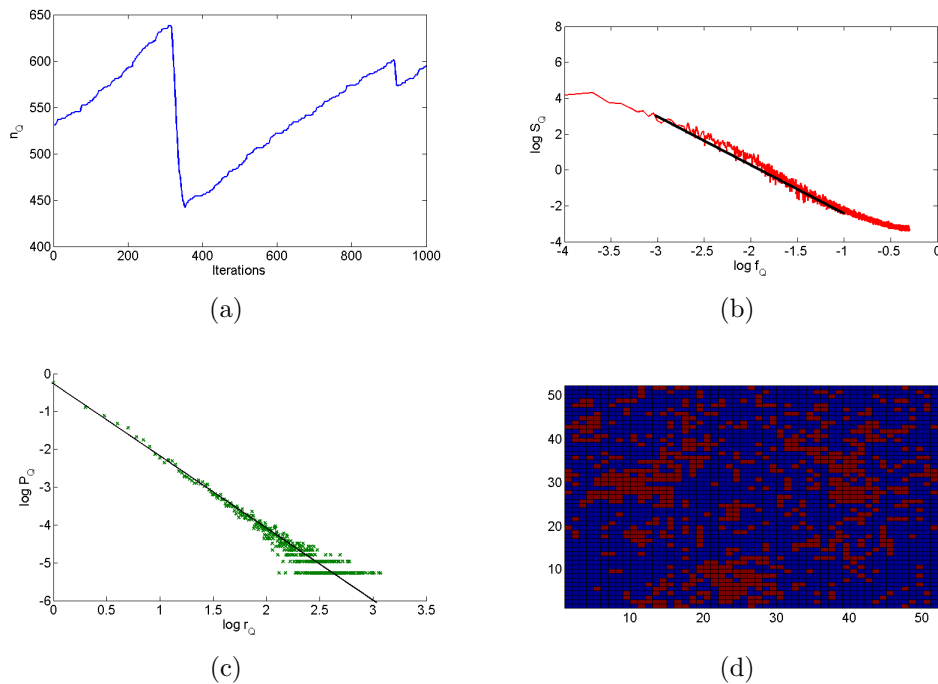


Figure 5.3: Results for ‘critical regime’: $\delta A = 10^{-4}$, $A_C = 1.0$, $A_R = 1.0$, $A_P = 0$: $a/b \approx 0.08$, $b \approx 10^{-4}$

The simulation is numerically close to the critical limits (5.1) and (5.2), with $a/b \approx 0.08$ and $b \approx 10^{-4}$. The structure plot corresponds to a period of non-activity. Clusters of quiescent site are evident across a range of sizes. The solid lines in Figures 5.3(a) and 5.3(c), are not fitted to the data, but rather show how the exponents are estimated. There are,

in general (see Section 2.1.1 and [10]), many issues when fitting power-law data. However, as our investigation is intended as an exploratory study, estimates of the exponents are sufficient to use.

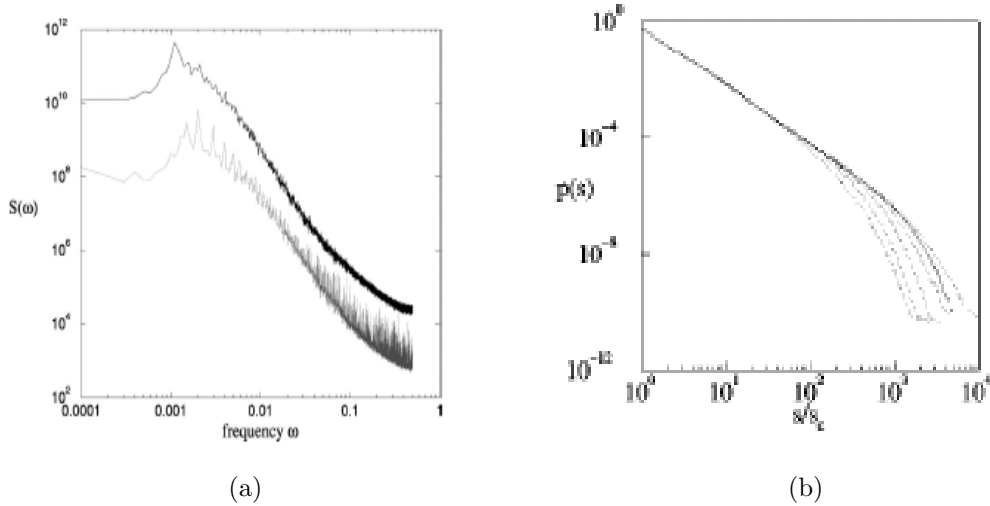


Figure 5.4: (a) $\log(S_Q)$ against $\log(f_Q)$, (b) $\log(P_Q)$ against $\log(r_Q)$ [34]

5.3 Simulation results in a meteorological region of parameter space

In this section we explore the cellular automation model in a region of parameter space that is thought to correspond to the physical region of the TCS discussed in Chapter 4. We relate to the model physics through the time scale separation $\delta A/A_C$ and the relative values of A_P , A_R and A_C . Figure 5.5 is thought to represent a parameter set that is closest to the physical constraints and has model time-scale ratio $\delta A/A = \frac{1}{32}$. This could, (for example), approximately correspond to $\tau_R \approx 45\text{min}$ and $\tau_C \approx 20\text{hrs}$. The choice of $A_P = 0.5$, means that sites with $A_{ij} \in (0.5, 1)$ can inter-convect. This corresponds to a moisture perturbation in a neighbouring site, triggering the top third of sites that have evolved in accordance with the threshold model.

The power-law relationship that was observed between S_Q and f_Q in Figure 5.3 is no longer evident. A strong peak in the power spectrum is present at $\log(f_Q) \approx -1.5$. This

arises due to the oscillatory component in the time signal of n_Q . The power-law relationship between P_Q and r_Q still weakly exists, with exponent $\beta \approx 2.0$; but is now only over one order of magnitude. The values of a/b and b are not as close to the critical limits as in Figure 5.3 at $a/b \approx 0.1$ and $b \approx 0.03$ respectively.

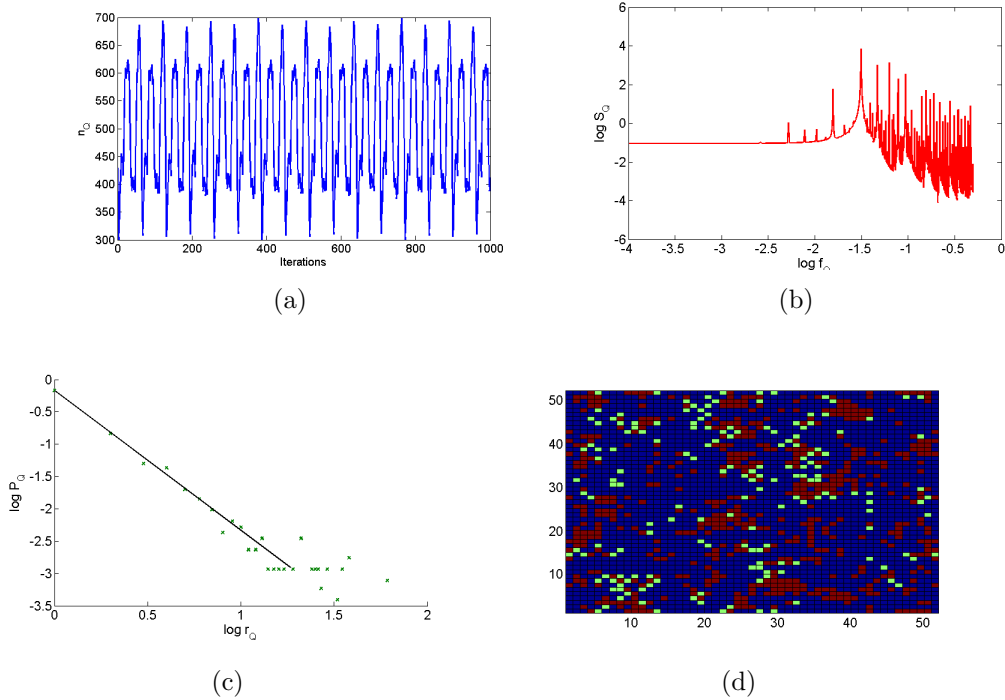


Figure 5.5: Results for typical meteorological parameter set: $\delta A = \frac{1}{32}$, $A_C = 1.0$, $A_R = 1.0$, $A_P = 0.5$: $a/b \approx 0.1$, $b \approx 0.03$

Figure 5.6 is thought to represent the lower bound of $\delta A/A$ that can be justified from the physical constraints. The results correspond to a regime of behaviour between the parameter sets used in Figures 5.3 and 5.5. A power-law relationship is observed between S_Q and f_Q , with a similar exponent to Figure 5.3 of $\alpha \approx 2.7$. However, it is less well defined and only over a regime of 1-1.5 orders of magnitude.

An oscillatory peak in the spectrum is again present as in Figure 5.5 when $\log(f_Q) \approx -2$. Since $\log(\frac{1}{32}) = -1.51$ and $\log(\frac{1}{96}) = -1.98$, it is thought that the oscillatory components can be directly related by $A_C/\delta A \approx f_{osc}$ where f_{osc} is a harmonic driving frequency. f_{osc} is physically representative of the auto-convection time-scale, (in absence of inter-

convection). The power-law relationship between P_Q and r_Q exists over an intermediate magnitude range, with exponent $\beta \approx 2.0$. The values of a/b and b are intermediate between Figure 5.3 and Figure 5.5.

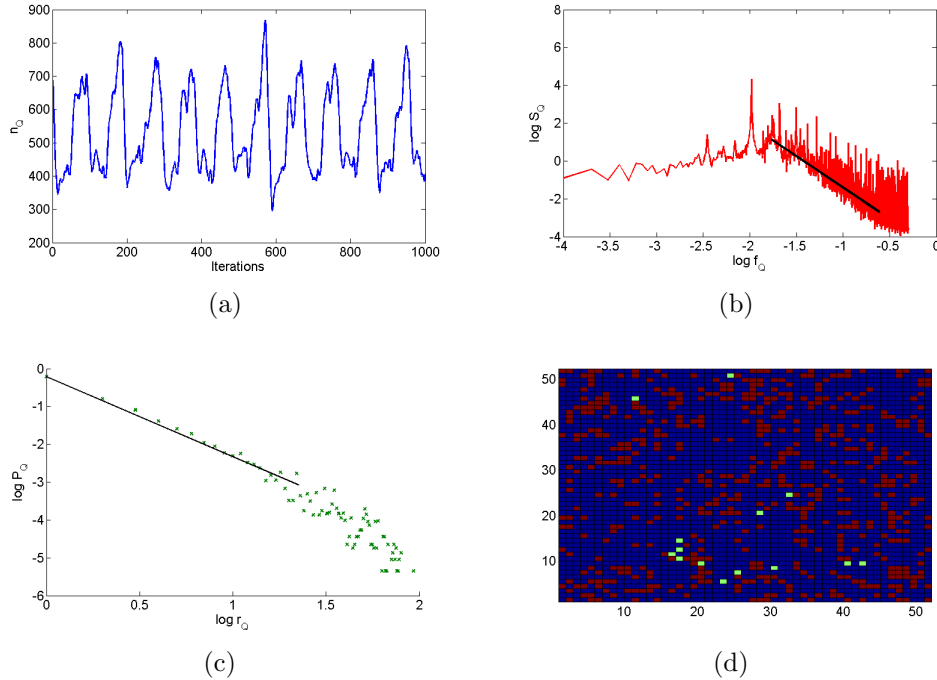


Figure 5.6: Results for lower bound upon time-scale separation: $\delta A = \frac{1}{96}$, $A_C = 1.0$, $A_R = 1.0$, $A_P = 0.5$: $a/b \approx 0.1$, $b \approx 0.01$

5.4 Relaxation parameterisations

This section investigates different relaxation parameterisations for the model. Relaxations to a fixed value, stochastic value and hybridisations with the original parameterisation are investigated. The cases studied are:

- $A_{ij} \rightarrow \kappa$ where κ is a constant.
- $A_{ij} \rightarrow c_1\kappa + c_2(A_{ij} - A_R)$ where $c_1, c_2 > 0$ and $c_1 + c_2 = 1$.
- $A_{ij} \rightarrow X$ where $X \in [-1/2, 0]$ is a stochastic variable.
- $A_{ij} \rightarrow c_3X + c_4(A_{ij} - A_R)$ where $c_3, c_4 > 0$ and $c_3 + c_4 = 1$.

5.4.1 Relaxation to fixed value and hybrid

Output for relaxing to a fixed value; $A_{ij} \rightarrow \kappa$, where $\kappa = -\frac{1}{4}$ is shown in Figure 5.7. The lattice is observed to synchronise. No inter-convection occurs and all sites auto-convect at the same time. The time-series n_Q is correspondingly a periodic step function, alternating between 0 and 2500 sites on the lattice being quiescent.

The hybrid relaxation; $A_{ij} \rightarrow c_3\kappa + c_4(A_{ij} - A_R)$ where $c_1 = c_2 = \frac{1}{2}$, $\kappa = -\frac{1}{4}$ is also observed to synchronise, having an output identical to Figure 5.7. This result indicates that a transition between the behaviour for the relaxation to a fixed value and the original parameterisation must exist for $c_1 \in (0, 0.5)$ and $c_2 \in (0.5, 1)$.

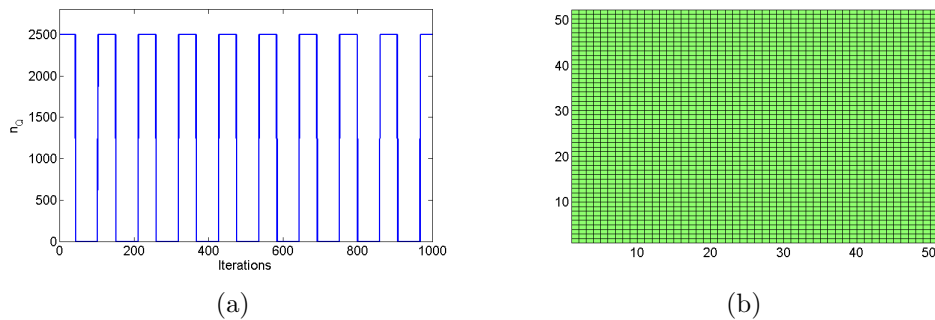


Figure 5.7: Results for relaxation to a fixed value: $\delta A = \frac{1}{96}$, $A_C = 1.0$, $A_R = 1.0$, $A_C = 0.5$

5.4.2 Relaxation to a stochastic value and hybrid

Figure 5.8 shows the result for the stochastic relaxation mechanism; $A_{ij} \rightarrow X$. The results are broadly similar to Figure 5.5 with similar values for α and β , where power-laws can be argued to exist, (values given in Table 5.1, Section 5.6). It is however suggested in Figure 5.8 that the relationship between P_q and r_Q is possibly not best described by a power-law. The power spectrum and quiescent cluster size plots are both smoother for the stochastic value relaxation than for the original mechanism. The harmonic peak in the power spectrum is wider in the stochastic value relaxation, as would be expected by introducing a random effect.

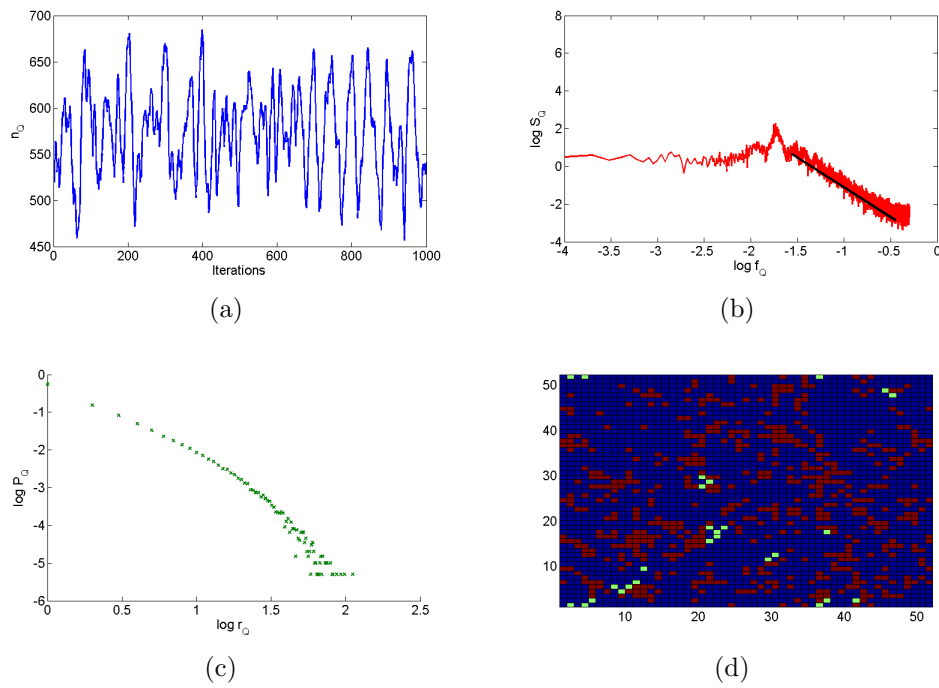


Figure 5.8: Results for relaxation to stochastic value: $\delta A = \frac{1}{96}$, $A_C = 1.0$, $A_R = 1.0$, $A_P = 0.5$:
 $a/b \approx 0.08$, $b \approx 0.01$

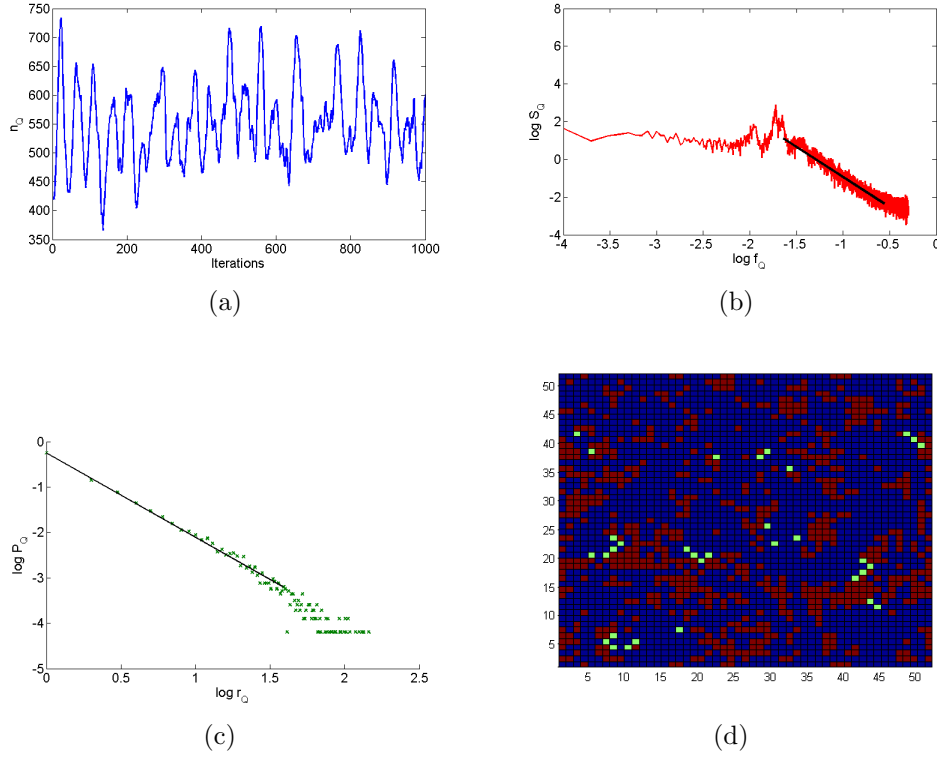


Figure 5.9: Results for relaxation to stochastic-hybrid value: $\delta A = \frac{1}{96}$, $A_C = 1.0$, $A_R = 1.0$, $A_P = 0.5$: $a/b \approx 0.07$, $b \approx 0.01$

Figure 5.9 shows the result for the hybrid stochastic relaxation mechanism; $A_{ij} \rightarrow c_3 X + c_4(A_{ij} - A_R)$, for $c_3 = c_4 = \frac{1}{2}$. It is observed that the power spectrum and cluster size plots are of intermediate character between Figure 5.5 and Figure 5.8, in agreement with what we would expect.

5.5 System size investigation

Using the stochastic-hybrid relaxation mechanism, the effect of increasing the system size upon the scale-invariant diagnostics is investigated. Figure 5.10 shows the relationship between $\log(r_Q)$ and $\log(P_Q)$ for lattice sizes of $L = 250$, $L = 50$ and $L = 10$. The power-law regime is observed to be approximately the same over all system sizes, with a robust exponent of $\beta \approx 1.8$. It was also observed that the power-spectrum relationship; $S_Q \propto f_Q^{-\alpha}$, does not change with system size.

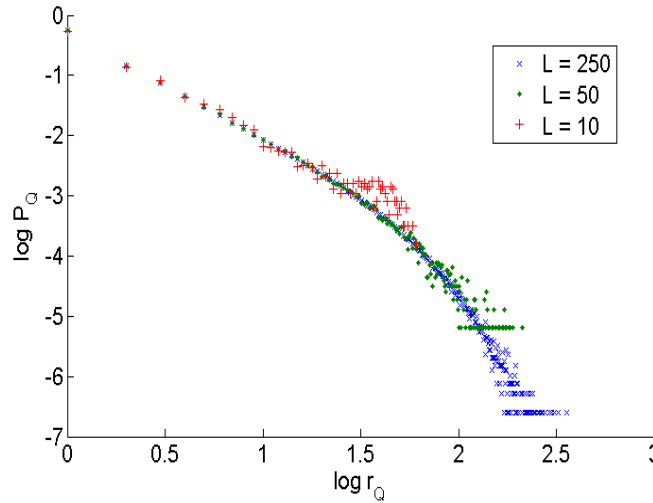


Figure 5.10: System size plots for $\log(r_Q)$ against $\log(P_Q)$: $L = 250$, $L = 50$, $L = 10$

It is interesting that the extent of the power-law regime does not differ greatly between system sizes, being approximately 1.5 orders of magnitude in each case. This suggests that a natural power-law regime for cluster-size appears to exist for the model parameter set that is independent of system size. In turn, this suggests that the results we have obtained for $L = 50$ are likely to be representative of simulations on greater size lattices. The larger system $L = 250$ does, however, support larger clusters - it is just that the regime where larger clusters exist does not follow a power-law relationship.

5.6 Summary of results

Primarily, this chapter has investigated the application of the DFF model to the TCS. This was done by identifying the parameters of the DFF model with the dynamical features of the TCS and then using parameter values which could be linked to the model physics outlined in Chapter 4. A feature of our investigation, was to adapt the original model to explore larger values of $\delta A/A_C$ and A_P . A range of relaxation parameterisations were then investigated. A summary of the model simulations in this chapter is given in Table 5.1. The exponents α and β correspond to estimates.

It was established that the typical meteorological parameter values (Figure 5.5) did not produce strongly distinct power law relationships in comparison to what is deemed the

critical limit of the system (Figure 5.3). The meteorological parameters with the greatest degree of time-scale separation that can be justified for the TCS (Figure 5.6), show promise of power-law relationships, albeit over a limited regime of about 1.5 orders of magnitude. It is therefore thought that the slower the ‘drive’ of the system, (i.e. how close $\delta A/A_C$ is to 0), the more distinct and large the regimes of power-law relationships will be.

Fig.	δA	A_C	A_P	Relaxation	α	β	a/b	b	Scaling regime
5.3	10^{-4}	1.0	0.0	$A_R = 1.0$	2.4	1.9	0.007	10^{-4}	2.5-3 MR for $S_Q \propto f_Q^{-\alpha}$, $P_Q \propto r_Q^{-\beta}$
5.5	$\frac{1}{32}$	1.0	0.5	$A_R = 1.0$	-	2.0	0.08	0.03	1MR for $P_Q \propto r_Q^{-\beta}$ (in- distinct)
5.6	$\frac{1}{96}$	1.0	0.5	$A_R = 1.0$	2.7	2.0	0.1	0.01	1.5 MR for $S_Q \propto f_Q^{-\alpha}$
5.7	$\frac{1}{96}$	1.0	0.5	κ	-	-	-	-	None (synchronised)
5.8	$\frac{1}{96}$	1.0	0.5	X	2.4	1.7	0.08	0.01	1.5 MR reg. for $S_Q \propto$ $f_Q^{-\alpha}$
5.9	$\frac{1}{96}$	1.0	0.5	$A_R = 1.0, X$	2.6	1.8	0.07	0.01	1.5 MR for $S_Q \propto f_Q^{-\alpha}$, $P_Q \propto r_Q^{-\beta}$

Table 5.1: Summary of simulation results from cellular automation model of TCS, (MR corresponds to ‘Magnitude Regime’ of power-law relationship)

The apparent robustness of the exponents α and β between the original relaxation, the stochastic relaxation and the stochastic-hybrid relaxation is encouraging. It provides scope for variations in the relaxation parameterisation that do not alter the scale-invariant diagnostic relationships to a large degree. The hybrid stochastic relaxation is thought to be the best physical representation of convective relaxation. This is because the reset value contains both an element of sensitivity to the state upon convection, and a stochastic element. The stochastic element can be viewed as representing physical processes that are not included in the simple cellular automation model, which are crucial if the model is to have any relevance to physical reality.

The numerical simulations carried out in this chapter have significance beyond the application of the DFF to the TCS. Notably, the numerical evaluation of the mean-field critical limits in Section 5.2.2 suggests that the parameters used by Sinha-Ray and Jensen

are numerically close to what would be expected for the system to be critical. This consolidates their conclusions which were based upon a comparison to the results of the SFF model.

The investigation of the relaxation mechanism to a fixed value is also thought to have wider consequences for the field of SOC. This mechanism is similar to in the OFC earthquake model (Section 2.3), with; $A_{ij} \rightarrow \kappa$ and $F_{ij} \rightarrow 0$ respectively. As stated in Section 2.3.3, the OFC model is observed to synchronise when periodic (rather than open) boundary conditions are introduced. Synchronisation was also observed for relaxation to fixed value in our model simulations of the TCS (Figure 5.7). It is therefore thought that the combination of periodic boundary conditions and a relaxation to a fixed value could potentially be a sufficient condition for a cellular automation algorithm to achieve synchronisation.

Chapter 6

Summary, future work and conclusions

6.1 Summary and discussion

This study has been concerned with answering the question: ‘Does SOC occur in the TCS?’. Chapters 3, 4 and 5 can be viewed as breaking this central question into 3 sub-questions:

- Chapter 3: Is there sufficient empirical evidence to link SOC to the TCS?
- Chapter 4: Can the necessary self-organised critical dynamical features of the TCS be identified?
- Chapter 5: Can the TCS be represented as a phenomenological cellular automation model?

We now summarise to what extent these questions have been answered.

Is there sufficient empirical evidence to link SOC to the TCS?

Chapter 3 gave an overview of how the empirical evidence for SOC in the TCS has developed over the past 10-15 years. We suggested that this could be viewed as showing a progression from: observing general scale-free behaviour in the atmosphere, to observing $1/f$ behaviour in variables linked to convective events; to directly identifying tropical

rainfall data with predictions from the theory of critical phenomena. It was argued that the direct identification with the theoretical predictions of critical phenomena makes the strongest case for SOC in the TCS, potentially providing stronger empirical evidence than what is available for the seismic system.

Can the necessary self-organised critical dynamical features of the TCS be identified?

The dynamical features of the TCS suspected of being responsible SOC were made explicit by comparing them to features of the granular and seismic system. It was suggested that a convective cell corresponds to a DOF, the condition for deep convective instability is a threshold and that a build up of boundary layer moist static energy represents energy storage. The cold pool development process was highlighted as a way of representing both the relaxation at a site of convection and the interaction (through the gust-front region) between DOF.

The threshold model, (although neglecting many physical features), is thought to be a solid representation of the forcing and energy storage phase of the TCS. It allows for a precise quantification of what the threshold in the TCS corresponds to and the estimation of a forcing/driving convective time-scale.

The cold pool exists over a finite time period. The separation in timescale between drive and relaxation/interaction for TCS is subsequently less pronounced than the granular and seismic systems. Moreover, unlike the granular and seismic systems, the relaxation of a DOF and the interaction between DOF can occur at different times when viewed as part of the cold pool development process. It is therefore thought that the cold pool relaxation/interaction is the weakest part of the model physics proposed to be self-organised critical. It is expected that future models may try to isolate other mechanisms when considering the organisation of the system.

Can the TCS be represented as a phenomenological cellular automation model?

The cellular automation model of the TCS developed in Chapter 5 was based upon an adaptation and an extension of an existing model - the DFF. As such, the model was not designed with clear meteorological diagnostics in mind. We suggested that the relationship between quiescent site cluster size and probability, could have a significance for the relationship between size and probability of convective storms.

A strength of our adaptation of the DFF model was that we were able to propose links between some of the model parameters and the suspected self-organised critical dynamical features outlined in Chapter 4. This included the degree of time-scale separation between the driving stage and the interaction stage and the strength of the cold pool perturbation.

It was established that what is deemed the critical limit of the DFF model, lies away from the region of parameter space that is associated with the TCS. However, smaller power-law regimes for both temporal and spatial diagnostics do exist for what is thought to be around the lower bound upon convective time-scale separation. These regimes are typically 1.5 orders of magnitude. It was found that introducing a stochastic element to the model did not appear to alter the power-law regimes that are observed. This is highly encouraging as many physical processes of the TCS are missing from the DFF model, and the stochastic element is partially representative of this.

6.2 Future work

As it stands, the cellular automation model developed for the TCS does not directly explain any of the empirical evidence outlined in chapter 3. It is expected that for this to be fully realised, a cellular automation model must be devised with specific meteorological diagnostics in mind. Given the limited number of cellular automation algorithms that have so far been shown to describe SOC this is likely to be a difficult task.

We propose that, using the threshold model, a tentative link can be made to the boundary layer time-series and power spectra of convective variables produced by Yano et. al [7], (Section 3.2.2, Figures 3.3(a) and 3.3(b)). This is done to show how meteorological diag-

nostics of SOC might be obtained in the future. A_{ij} at a fixed lattice point is outputted throughout the simulation and substituted for the time variable t , in the threshold model level 1 equations (4.26) and (4.27). As A_{ij} is in the interval $A_{ij} \in [-0.5, 1)$, it is scaled to correspond to time in the interval $t \in [0, \tau_C)$ hours, where $\tau_C = 12.5$ hrs, in accordance with the original value obtained in the threshold model. From this, an approximate ‘time series’ of boundary layer variables can be generated. This is shown for q_1 in 6.1(a) using the stochastic hybrid relaxation mechanism. $\delta A/A = \frac{1}{32}$ is chosen, and given the choice τ_C corresponds to $\tau_R \approx 30$ mins. A power spectrum for q_1 , S_{q_1} can subsequently be determined using the same method as in Chapter 5.

The time-series of q_1 indicates that approximately 1-2 convective events occur in a 24 hour period. This consolidates our interpretation of the cellular automation model parameters in terms of τ_C and τ_R . The power spectrum is very noisy, although there are hints that a power-law relationship, with an approximate exponent $\alpha \approx 1.7$ exists over 2 orders of magnitude. This is slightly outside the range for q_1 given in [7], which corresponded to; $\alpha \in [0.8, 1.4]$.

It is believed that this is not the best diagnostic of a self-organised critical system as it is a property of a DOF, rather than the system as a whole. Nevertheless, it is still a useful result as it can potentially provide a way of thinking about the data in [7], which has no good previous explanation. It is envisaged that future work upon models of the TCS as self-organised critical system should aim to produce power-law relationships that are emergent properties of the system.

6.3 Conclusions

We conclude that the empirical evidence for elements of SOC in the TCS is very strong. It is thus thought that the emphasis should be placed upon developing a phenomenological model of the TCS that is able to anticipate the scale-free behaviour that arises in the system.

We believe that the main unresolved issues in the model physics that we have explored relate to; the finite time-scale separation between the driving and the relaxation stages of

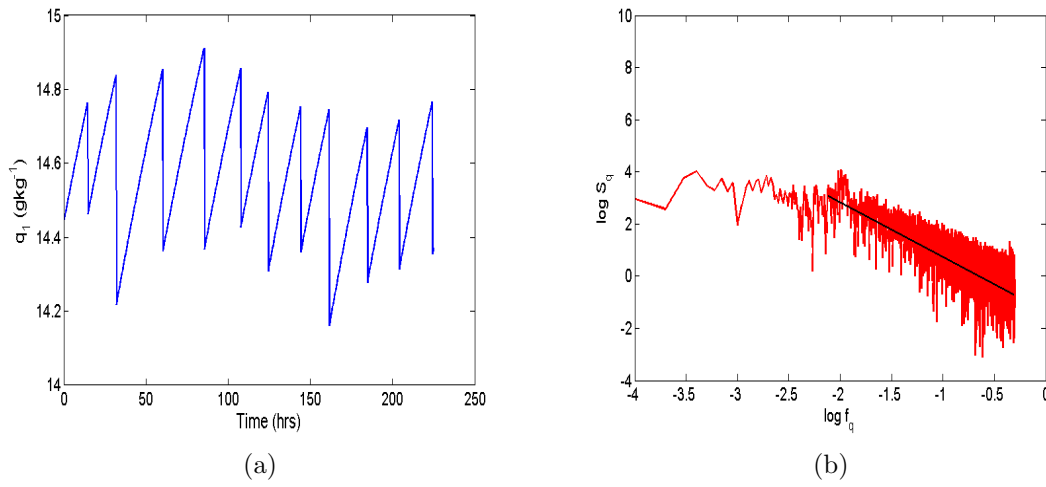


Figure 6.1: Results for q_1 : $\delta A = \frac{1}{32}$, $A_C = 1.0$, $A_R = 1.0$, $A_P = 0.5$: (a) Simulation time-series for q_1 , (b) $\log(S_{q_1})$ against $\log(f_{q_1})$

the dynamics of the TCS; and the nature of the interaction mechanism between DOF. The cold-pool development process is central to both these issues, and we expect that future work that is done upon the subject will focus upon a re-formulation of this, or explore other possible interaction mechanisms. Despite these issues, we believe that we have been largely successful in our identification of the dynamical features of the TCS with what is expected of a self-organised critical system.

The cellular automation model that was developed is thought to be an encouraging attempt at modelling the TCS as a self-organised critical system. For the first time, scale-free behaviour has been linked to a phenomenological model of the dynamics of the system. We have also shown that, through the relaxation parameterisation investigation, our model is robust to simple modifications. This has important consequences for its application to physical reality. The study is however, unable to directly reproduce the details of the empirical evidence for SOC in the TCS. We conclude that for this to be fully realised, a model must be devised with specific meteorological diagnostics in mind.

Appendix A

Model Simulation

A.1 Overview

The cellular automation model is constructed using the C++ programming language. Matlab is used for graphical output and post-processing. The age and status matrices, \underline{A} and \underline{B} correspond to 2 dimensional arrays of size $(L+2) \times (L+2)$. The periodic boundary conditions are implemented by copying the first interior rows and columns to each corresponding opposite lattice boundary after each iteration. This defines neighbouring points correctly and consistently. The central $L \times L$ region therefore corresponds to the ‘active’ region of the automation algorithm. The program code follows the algorithm outlined in Section 5.1.2. The inbuilt pseudo-random number generator *srand* is used to generate the initial conditions and stochastic reset relaxation mechanism.

A.2 Data sampling

Before sampling data, the simulation is iterated for $10(A_C/\delta_A)$ iterations. This number ensures that the critical state, (if it exists), is likely to have been obtained, (see section 5.2.2). A total sampling interval of 10^7 iterations is used for each data set. This is chosen to ensure that plot (c) has enough data. The data for plots (a), (b) and (d) are outputted at the middle of the total sampling interval.

A summary of the procedure used for each plot is as follows:

- (a) Time-series for n_Q : These are displayed over a output interval of 1000 iterations, taken 5×10^6 iterations into the sampling interval. The size of 1000 iterations was chosen because the definition of features is clear for the parameter sets used in the study.
- (b) S_Q against f_Q : The Fourier transform of n_Q is implemented using the inbuilt fast Fourier transform function in Matlab. An output interval of 10,000 iterations is used, corresponding to a frequency domain of $f_Q \in [\frac{1}{10,000}, \frac{1}{2}]$. The Fourier transform of n_Q is then averaged over 5 output intervals. This is found to produce the smoothest spectra for S_Q .
- (c) r_Q against P_Q : After every 10,000 iterations the frequency of cluster structures for each size that exists are counted and stored. This corresponds to 1000 ‘counts’ of the lattice in the total sampling interval. At the end of the total sampling interval the frequency data is used to assess the probability for a given cluster size. The program code for counting the cluster sizes in the lattice was based upon Fortran code written by Dr. Robert Plant. (The original code was intended for counting cloud structures).
- (d) Example of lattice structure plot: This is produced by outputting the matrix $\underline{\underline{B}}$ where suppressed, quiscent and active sites are stored as 0, 1, and 2 respectively. The Matlab graphic *pcolor* is used to produce the ‘checkerboard effect’.

Bibliography

- [1] P. BAK: How Nature Works: The Science of Self-Organised Criticality, *Spring-Verlag, New York*, (1996).
- [2] P. BAK, C. TANG AND K. WISSENFELD: Self-Organised Criticality: An explanation of $1/f$ Noise, *Physical Review Letters*, **59**, 381-384, (1987).
- [3] J. YEOMANS: Statistical Mechanics of Phase Transitions, *Oxford Science Publications*, (1992).
- [4] H. JENSEN: Self-Organised Criticality: Emergent Complex Behaviour in Physical and Biological Systems, *Cambridge Lecture Notes in Physics*, (1998).
- [5] VATTAY AND HARNOS: Scaling behaviour in Daily Air Humidity Fluctuations, *Physical Review Letters*, **73**, 768-771, (1994).
- [6] O. PETERS AND K. CHRISTENSEN: Rain: Relaxations in the Sky, *Physical Review Letters*, **66**, 1-9,(2002).
- [7] J. YANO, R. BLENDER, C. ZHANG AND K. FRAEDRICH: $1/f$ Noise and Pulse-like Events in the Tropical Atmospheric Surface Variabilities, *Q.J.R. Meteorological Society*, **130**, 1697-1721, (2003).
- [8] O. PETERS AND D. NEELIN: Critical phenomena in atmospheric precipitation, *Nature-Physics*, **2**, 393-400, (2006)
- [9] A. TOMPKINS: Organisation of Tropical Convection in Low Vertical Wind Shears: The Role of Cold Pools, *Journal of the Atmospheric Sciences*, **58**, 1650-1672, (2001).
- [10] A. CLAUSET, C. SHALIZA AND M. NEWMAN: Power-law distributions in empirical data, (*pre-print*), (2008).

- [11] <http://population.mongabay.com>
- [12] <http://en.wikipedia.org/wiki/Kochsnowflake>
- [13] <http://www.electricalnoise.net>
- [14] M. WEISSMAN: $1/f$ noise and other slow, nonexponential kinetics in condensed matter, *Reviews of Modern Physics*, **60**, 537-571, (1988).
- [15] V. FRETTE, K. CHRISTENSEN, A. MALTHER-SOERENSSON, J. FEDER, T. JOESANG, AND P. MEAKIN: Avalanche Dynamics in a Pile of Rice, *Nature*, **379**, 49-52, (1996).
- [16] <http://www.cmth.ph.ic.ac.uk/people/k.christensen/images/rice>
- [17] C. RHODES AND R. ANDERSON Power laws governing epidemics in isolated populations, *Nature*, **381**, 600602, (1996).
- [18] Z. OLAMI, H. JACOB AND K. CHRISTENSEN: Self-Organised Criticality in a Continuous, Nonconservative Cellular Automaton Modelling Earthquakes, *Physical Review Letters*, **68**, (1992).
- [19] <http://www.bgs.ac.uk/>
- [20] <http://www.rmets.org/cloudbank/index.php>
- [21] K. EMMANUEL: Dynamical Theories of Tropical Convection *Australian Meteorological Magazine*, **37**, 3-10, (1989).
- [22] R. HOUZE: Cloud Dynamics, *International Geophysics*, **53**, (1994).
- [23] A. ARAKAWA AND W. SCHUBERT: Interaction of a Cumulus Cloud Ensemble with the Large-Scale Environment: Part I, *Journal of the Atmospheric Sciences*, **31**, 674-701, (1973).
- [24] K. EMMANUEL: Atmospheric Convection, *Oxford University Press*, (1994).
- [25] H. KUO: Further studies of the parameterisations of the influence of cumulus clouds on the large-scale flow, *Journal of the Atmospheric Sciences*, **31**, 1232-1240, (2004).
- [26] D. NEELIN, O. PETERS, J. LIN, K. HALES AND C. HOLLOWAY: Rethinking convective quasi-equilibrium observational constraints for stochastic convection schemes in climate models, *Philosophical Transactions, Series A*, 2581-2604, (2008).

- [27] B. COHEN AND G. CRAIG: The time response of a convective cloud ensemble to a change in forcing, *Q.J.R. Meteorological Society*, **130**, 933-44, (2004).
- [28] L. DAVIES: Phd thesis: Self-organisation of Convection as a Mechanism for Memory, *University of Reading*, (2008).
- [29] <http://www.newscientist.com/article.ns?id=dn2241>
- [30] M. YANAI, S. ESBENSEN AND J. CHU: Determination of Bulk Properties of Tropical Cloud Clusters from Large-Scale Heat and Moisture Budgets *Journal of the Atmospheric Sciences*, **30**, 612-624, (1973).
- [31] W. SCHUBERT: A Retrospective View of Arakawa's Ideas on Cumulus Parameterisation: *General Circulation Model Development: Past, Present and Future*, (2000).
- [32] A. BETTS: Convection in the Tropics, *Meteorology over the Tropical Oceans*, 105-132, (1978).
- [33] <http://isccp.giss.nasa.gov/products/browsed2.html>
- [34] P. SINHA-RAY AND H. JENSEN: Forest-fire Models as a Bridge Between Different Paradigms in Self-Organised Criticality, *Physical Review Letters*, **62**, 3215-3218, (2000).
- [35] B. DROSSEL AND F. SCHWABEL: Self-Organised Critical Forest Fire Model, *Physical Review Letters*, **69**, 1629-1633, (1992).
- [36] K. CHRISTENSEN, H. FLYVBJERG, AND Z. OLAMI: Self-Organised Critical Forest-Fire Model: Mean-field Theory and Simulation Results, *Physical Review Letters*, **71**, 2737-2740, (1993).